高感度分子間力顕微鏡による細胞間接着分子ネクチン・カドヘリンの1分子間結合力計測

Bond strength measurement between the single cell adhesion molecules, nectin and cadherin, using high sensitive Intermolecular Force Microscopy

Department of Mesoscopic Materials Science, Graduate School of Materials Science, Nara Institute of Science and Technology

Doctoral dissertation Jan, 2007

Yoshikazu Tsukasaki

Index

0. Summary

Nectins and cadherins, members of cell adhesion molecules (CAMs), are the primary mediators for various types of cell-cell junctions. Here, intermolecular force microscopy (IFM) with force sensitivity at sub-piconewtons is used to characterize the extracellular *trans*-interactions between paired nectins and paired cadherins at a single molecule level. Three and four different bound states between paired nectins and paired cadherins are respectively identified and characterized based on bond strength distributions where each bound state has a unique lifetime and bond length. The results indicate that multiple domains of nectins act uncooperatively, as a zipper-like multiply bonded system whereas those of cadherins act cooperatively, as a parallel-like multiply bonded system, consistent with a "fork initiation and zipper" hypothesis for the formation of cell-cell adhesion. The observed dynamic properties among multiple bonds are expected to be advantageous such that nectins search adaptively in the cell-cell exploratory recognition process while cadherins slowly stabilize in the cell-cell zippering process.

1. General introduction

1.1. Background

Cells in multicellular organisms have the ability to recognize and adhere to their neighboring cells, and to form intercellular junctions. These play essential roles in various cellular processes, including morphogenesis, differentiation, proliferation and migration(Takeichi 1991; Gumbiner 1996; Vleminckx and Kemler 1999; Tepass, Truong et al. 2000). Furthermore, these are also important in the continued maintenance of tissue structure and integrity, high correlated with the invasiveness of some types of tumors (**Figure 1**). Intercellular junctions are generally associated with the actin cytoskeleton, and this strengthens intercellular adhesion. In polarized epithelial cells, cell-cell adhesion is mediated through a junctional complex comprising tight junctions (TJs), adherence junctions (AJs) and desmosomes (DSs) (**Figure 1**)(Farquhar and Palade 1963). These junctional structures are typically aligned from the apical to basal sides, although DSs are independently distributed in other areas. TJs are likely to serve as a barrier that prevents solutes and water from passing through the paracellular pathway and as a fence between the apical and basolateral plasma membranes in

epithelial cells(Tsukita and Furuse 1999; Tsukita, Furuse et al. 2001). AJs play key roles in the formation and maintenance of TJs and DSs and furthermore in concentration of many biologically active molecules, such as membrane receptors, signaling molecules and oncoproteins(Tsukita, Nagafuchi et al. 1992; Aberle, Schwartz et al. 1996; Anastasiadis and Reynolds 2000; Gumbiner 2000; Nagafuchi 2001). TJs also concentrate tumor suppressor proteins and cell polarity proteins(Tsukita and Furuse 1999; Tsukita, Furuse et al. 2001).

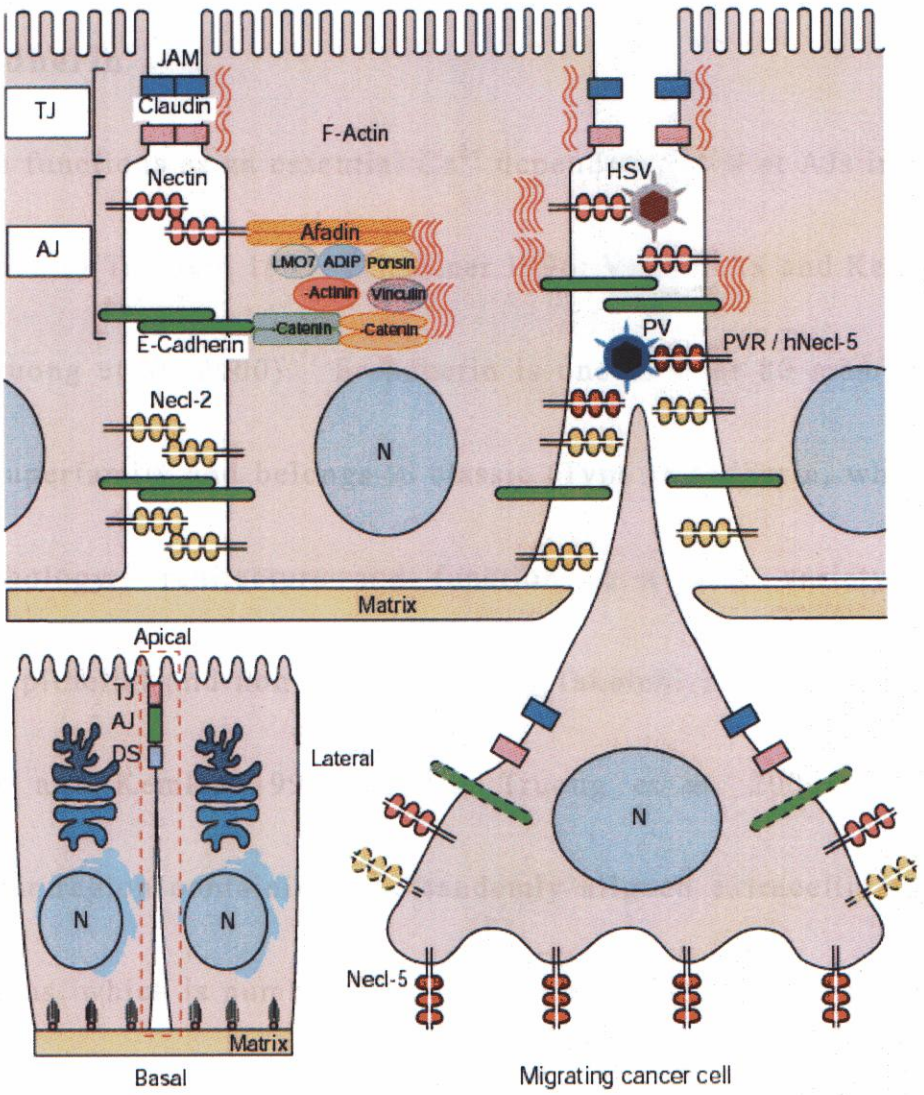

Figure 1 Molecular basis for AJs and TJs and migrating cancer cell

The junctional complex, which consists of TJs, AJs and DSs, localizes at the lateral membrane and is undercoated with F-actin in epithelial cells. JAM and claudin localize at TJs. Nectin localizes at AJs. E-Cadherin localizes at AJs and the lateral plasma membrane. Nectins associate with cadherins through three putative connector units: a ponsin-vinculin unit, an ADIP-a-actinin unit, and a LMO7-a-actinin unit. Nectin-like molelcule (Necl-2) localizes at the basolateral plasma membrane, although not in the specialized cell–cell junctions, such as AJs, TJs, and desmosomes. During migration of cancer cells, Nectin-like molelcule (Necl-5) is up-regulated. In contrast, E-cadherin and Necl-2 are down-regulated (shown by dashed lines). Nectin-like molelcule (Necl-5) localizes at leading edges of migrating cells and enhances cell motility. Nectin serves as a receptor for HSV. Nectin-like molelcule (Necl-5) serves as a receptor for poliovirus (PV). The red dashed box in the lower panel corresponds to the upper panels.

1.2. Cadherin

E-cadherin functions as an essential Ca^{2+} dependent CAM at AJs in epithelial cells (**Figure 1**)(Takeichi 1991; Gumbiner 1996; Vleminckx and Kemler 1999; Tepass, Truong et al. 2000). E-cadherin is one of over 80 members in the cadherin superfamily and belongs to classic (Type I) cadherin, which affects cell morphology, architecture and function in a wide variety of cells, including epithelial and non-epithelial cells(Takeichi 1991; Gumbiner 1996; Vleminckx and Kemler 1999; Tepass, Truong et al. 2000). It has an extracellular region containing five tandemly aligned extracellular cadherin (EC) domains, which is numbered EC1 at outermost N-terminal to EC5 in the proximity of transmembrane region (TM) (**Figure 2** and **Figure 3**)(Yagi and Takeichi 2000; Boggon, Murray et al. 2002). Its extracellular adhesion activity, a critical component of cell-cell adhesions(Gumbiner 2005), has been investigated in numerous studies, such as mutational experiments(Nose, Tsuji et al. 1990; Tamura, Shan et al. 1998), binding kinetics(Chappuis-Flament, Wong et al. 2001; Perret, Benoliel et al. 2002), force measurements(Sivasankar, Brieher et al. 1999; Chu, Eder et al. 2006), electron microscopy(Pertz, Bozic et al. 1999) and structural studies(Boggon,

Murray et al. 2002). Several hypotheses for extracellular adhesion have been proposed, however, the molecular mechanism has continued to be controversial (**Figure 4**)(Gumbiner 2005; Troyanovsky 2005). The 'strand dimer zipper' hypothesis is based on the crystal structure of only N-terminal EC1 domain of N-cadherin, which first appears in the vertebrate nervous system (**Figure 4a**)(Shapiro, Fannon et al. 1995). Two adhesive interfaces on EC1 were observed; the first one was thought to mediate *cis*-interaction, in which the Trp(W)2 residue of each subunit inserts into a hydrophobic pocket on the other EC1 subunit; the second putative adhesive interface for *trans*-interaction is the surface that surrounds the conserved HAV sequence. The Trp(W)2-mediated *cis*-interaction has been supported by numerous biochemical evidence(Brieher, Yap et al. 1996; Ozawa and Kemler 1998; Tamura, Shan et al. 1998; Takeda, Shimoyama et al. 1999; Shan, Tanaka et al. 2000; Klingelhofer, Laur et al. 2002; Ozawa 2002). However, the putative adhesive interface for *trans*-interaction that surrounds the HAV sequence has not been supported by mutagenesis studies(Kitagawa, Natori et al. 2000; Laur, Klingelhofer et al. 2002; Renaud-Young and Gallin 2002). Thus, it is thought that the putative adhesive interface for *trans*-interaction that

surrounds the HAV sequence probably arose from crystal packing interactions. Recently, a crystal structure for the whole EC domains (EC1-EC5) of the C-cadherin, which has been shown to be critical for maintaining adhesion between the blastomeres of the *Xenopus* blastula and be required for the normal movements of gastrulation, was reported (**Figure 3**)(Boggon, Murray et al. 2002). A revised hypothesis has been proposed that the Trp(W)2-mediated adhesive interface mediate the *trans*-interaction instead of the *cis*-interaction (**Figure 4b**)(Boggon, Murray et al. 2002). The hypothesis for *trans*-interaction mediated by Trp(W)2 has also been proposed for the desmosomal glycoproteins as a result of an electron microscopic study of desmosomes(He, Cowin et al. 2003). An alternative hypothesis for both *cis*- and *trans*-interaction has also been proposed based on the crystal structure for EC1-2 of E-cadherin(Nagar, Overduin et al. 1996) and electron microscopy studies of multimerized chimera cadherins (**Figure 4c**)(Pertz, Bozic et al. 1999). In this hypothesis, *cis*-interaction occurs at the Ca^{2+} binding site between EC1 and EC2, and the Trp(W)2 residue inserts into its own pocket to activate *trans*-interaction interface with another surface of EC1. On the other hand, biophysical and biochemical studies showed that all EC domains

involved *trans*-interaction interface and indicated important roles for the other EC domains in the adhesive interaction of *trans*-interaction(Sivasankar, Brieher et al. 1999; Chappuis-Flament, Wong et al. 2001; Zhu, Chappuis-Flament et al. 2003). This hypothesis entails a much more extensive overlap between all EC domains (**Figure 4d**). Further support for this model comes from a study of L-CAM (chicken E-cadherin), which showed that EC1 is not essential for adhesive interaction(Renaud-Young and Gallin 2002). Further work is needed to integrate these models and to explain the structure of the adhesive interaction.

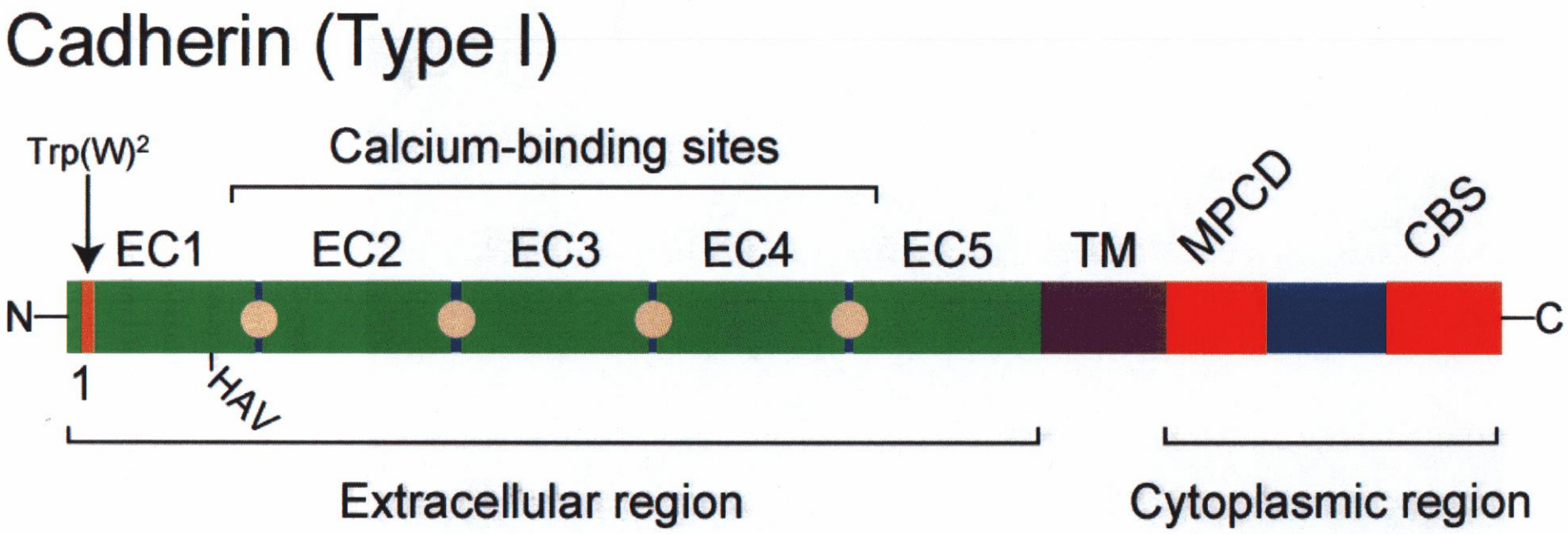

Figure 2 Molecular structure of cadherin (Type I)

Classic (Type I) Cadherin has an extracellular region containing five tandemly aligned extracellular cadherin domains (EC; numbered EC1 to EC5), a single transmembrane region (TM) and a cytoplasmic region. The extracellular region contains four groups of calcium-binding sites (yellow circles) positioned between adjacent EC domains. An arrow (Trp(W)2) indicates the position of the Trp(W) residue predicted to mediate cadherin homodimerization and conserved in classic (Type I) and desmosomal cadherins. HAV indicates the position of HAV sequence conserved in classic (Type I) cadherin. N- represents anino termini. -C represents carboxyl termini.

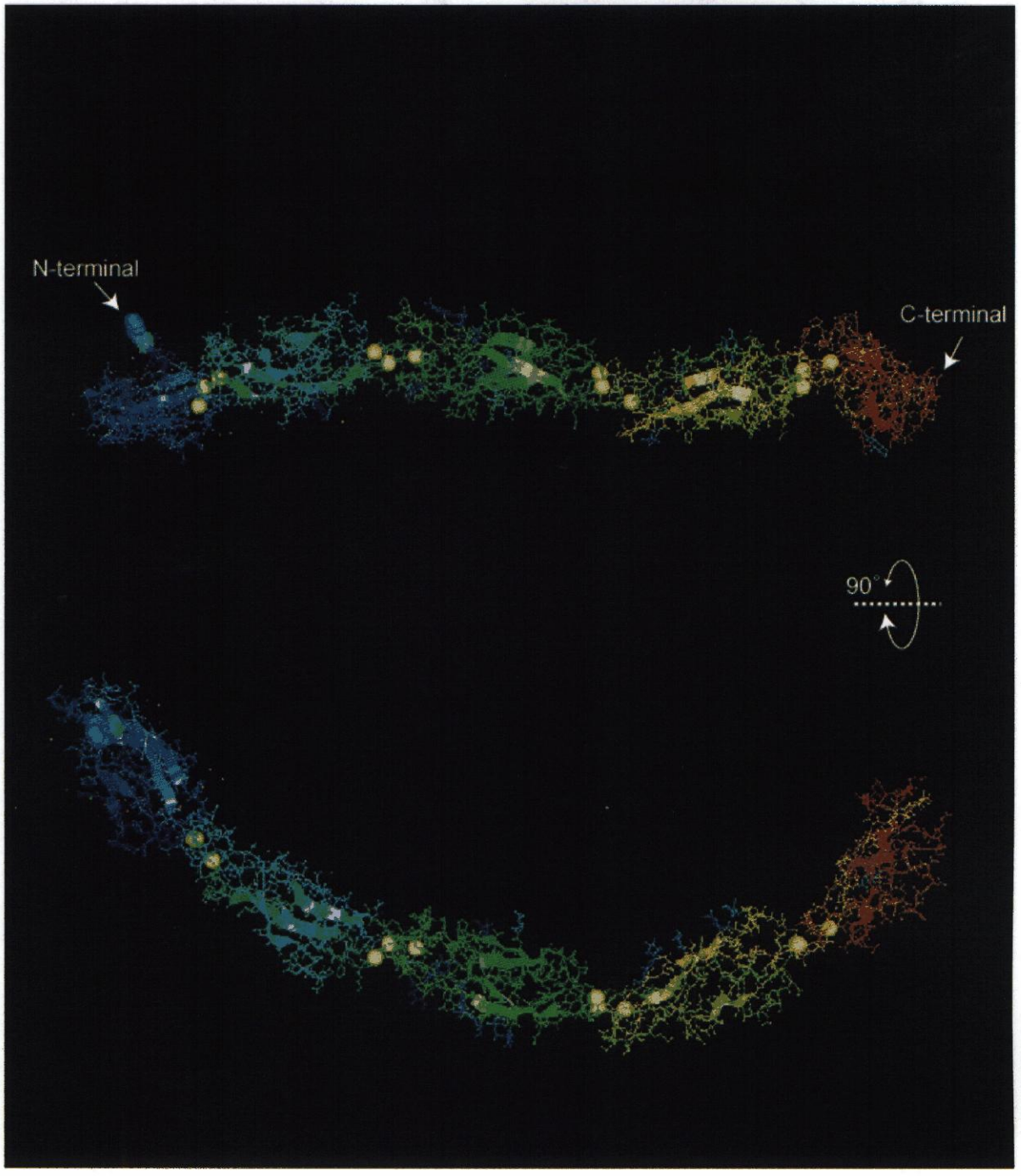

Figure 3 Crystal structure of C-cadherin

Ball stick and ribbon representation of C-cadherin ectodomain (EC1-EC5). (**Lower**) View from 90° away from upper view. Trp(W)2 residue are shown in ball representation. Yellow ball represents calcium ions. Membrane distal N-terminal and membrane proximal C-terminal is shown white arrows.

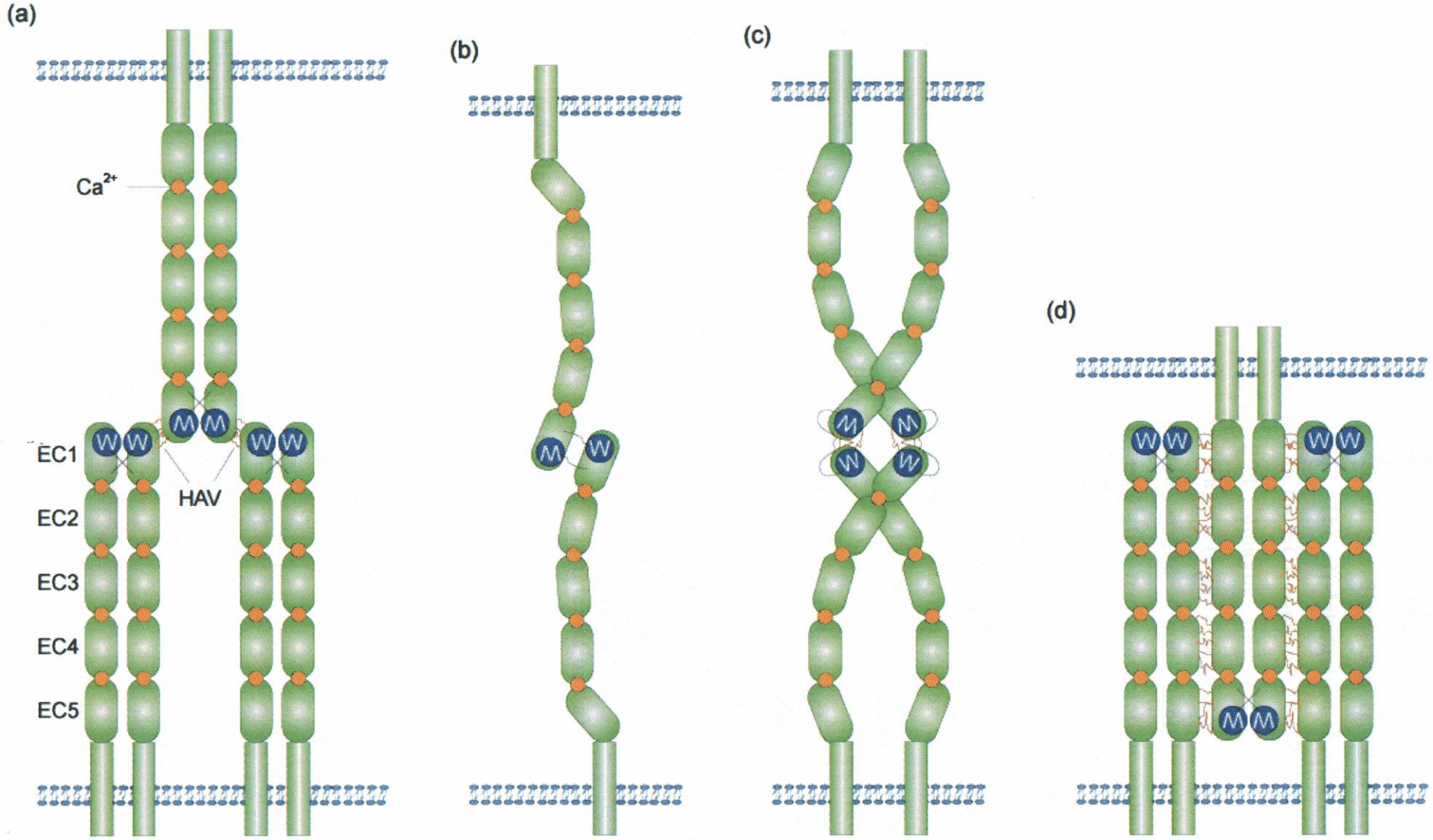
(a)
Ca2+
EC1
EC2
EC3
EC4
EC5
HAV
(b)
(c)
(d)

Figure 4 Several hypotheses of cadherin interaction

(**a**) Strand dimer zipper hypothesis composed of interdigitating Trp(W)2-mediated *cis*-interaction(Shapiro, Fannon et al. 1995). The *cis*-interaction results from the reciprocal insertion of the Trp(W)2 residue in the EC1 domain of one subunit into a hydrophobic pocket (**Blue**) of the EC1 domain of the other subunit. *Trans*-interaction occurs at a different site (**shown in red**), that surrounds the HAV sequence. (**b**) Revised Trp(W)2-mediated strand dimer hypothesis(Boggon, Murray et al. 2002), in which Trp(W)2 mediates *trans*-interaction rather than *cis*-interaction. As in strand dimer zipper hypothesis (**a**), there is still a reciprocal insertion of the Trp(W)2 residue into the hydrophobic pocket (**Blue**) between EC1 domains. However, these involve in only *trans*-interaction interface. (**c**) Hypothesis that invokes a Ca^{2+}-dependent *cis*-interaction interface, and intramolecular Trp(W)2 insersion to activate the *trans*-interaction interface(Pertz, Bozic et al. 1999). In this hypothesis, the Ca^{2+}-binding sites between the EC1 and EC2 mediate *cis*-interaction. Insertion of the Trp(W)2 residue into the hydrophobic pocket on EC1 (**Blue**) is intramolecular and, rather than mediating interaction interface, this insertion changes the conformation of the surface of EC1 (**Blue**), which activates *trans*-interaction interface. (**d**) A hypothesis that invokes extensive overlap between Trp(W)2-mediated *cis*-dimers(Sivasankar, Brieher et al. 1999; Chappuis-Flament, Wong et al. 2001; Zhu, Chappuis-Flament et al. 2003). This hypothesis implicates the other EC domains as well as EC1 in the formation of *trans*-interaction. Here, Trp(W)2 mediates *cis*-interaction as in model **a**. However, *trans*-interaction interface (**Blue**) involves many of the EC domains. Ca^{2+} ions are indicated by yellow circles.

1.3. Nectin

Nectin is another novel CAM at Ajs in epithelial cells (**Figure 1**). Nectins, which comprise a family of at least four members, nectin-1, -2, -3 and nectin-4, play key roles in the formation of AJs in epithelial cells and fibroblasts cooperatively with E-cadherins(Takahashi, Nakanishi et al. 1999; Satoh-Horikawa, Nakanishi et al. 2000; Tachibana, Nakanishi et al. 2000), the formation of synapses cooperatively with N-cadherin(Mizoguchi, Nakanishi et al. 2002), and the formation of Sertoli cell-spermatid junctions of the testis independently of cadherins(Ozaki-Kuroda, Nakanishi et al. 2002). Nectin has an extracellular region containing three tandemly aligned Ig-like domains (**Figure 5**)(Takai and Nakanishi 2003). Its extracellular activity also has been investigated and compared with those of cadherins by mutational experiments(Miyahara, Nakanishi et al. 2000; Reymond, Fabre et al. 2001), binding kinetics(Yasumi, Shimizu et al. 2003) and force measurements(Martinez-Rico, Pincet et al. 2005) although no information of crystal structure. In contrast to cadherins, the extracellular activity of nectins is Ca^{2+} independent (Aoki, Koike et al. 1997; Takahashi, Nakanishi et al. 1999; Miyahara, Nakanishi et al. 2000; Satoh-Horikawa, Nakanishi et al.

2000). However, in common with E-cadherin, it is likely that nectin also has two types of interactions, *cis*- and *trans*-interactions(Lopez, Aoubala et al. 1998; Miyahara, Nakanishi et al. 2000; Satoh-Horikawa, Nakanishi et al. 2000; Momose, Honda et al. 2002). Analysis of point and truncated mutants of nectin reveals that each nectin family member forms a homo-*cis*-dimer but not a hetero-cis-dimer(Satoh-Horikawa, Nakanishi et al. 2000). Each member also forms a homo-*trans*-dimer(Aoki, Koike et al. 1997; Lopez, Aoubala et al. 1998; Takahashi, Nakanishi et al. 1999; Miyahara, Nakanishi et al. 2000; Satoh-Horikawa, Nakanishi et al. 2000; Reymond, Fabre et al. 2001; Momose, Honda et al. 2002). Nectin-3, however, can form a hetero-*trans*-dimer with either nectin-1 or nectin-2, and these hetero-*trans*-dimers are much higher affinity than homo-*trans*-dimers(Satoh-Horikawa, Nakanishi et al. 2000; Yasumi, Shimizu et al. 2003). In this respect, nectins differ from cadherins, which form mainly homo-*trans*-dimers(Takeichi 1991; Gumbiner 1996; Vleminckx and Kemler 1999; Tepass, Truong et al. 2000; Yagi and Takeichi 2000; Angst, Marcozzi et al. 2001). A mutant of nectin lacking the second Ig-like domain does not form a cis-dimer, indicating that the second Ig-like domain is

necessary for the formation of the *cis*-interaction(Momose, Honda et al. 2002). Nevertheless, a fragment of the first Ig-like domain can mediate a *cis*–interaction(Krummenacher, Baribaud et al. 2002). This domain is thus also likely to be involved in the formation of the *cis*-interaction(Fabre, Reymond et al. 2002; Krummenacher, Baribaud et al. 2002). In addition, the first Ig-like domain is necessary for mediating the *trans*-interaction(Aoki, Koike et al. 1997; Lopez, Aoubala et al. 1998; Takahashi, Nakanishi et al. 1999; Miyahara, Nakanishi et al. 2000; Satoh-Horikawa, Nakanishi et al. 2000; Reymond, Fabre et al. 2001; Momose, Honda et al. 2002). It is suggested that the second and the third Ig-like domains also involved *trans*-interaction(Yasumi, Shimizu et al. 2003). Thus, the details of molecular mechanism have continued to be unclear.

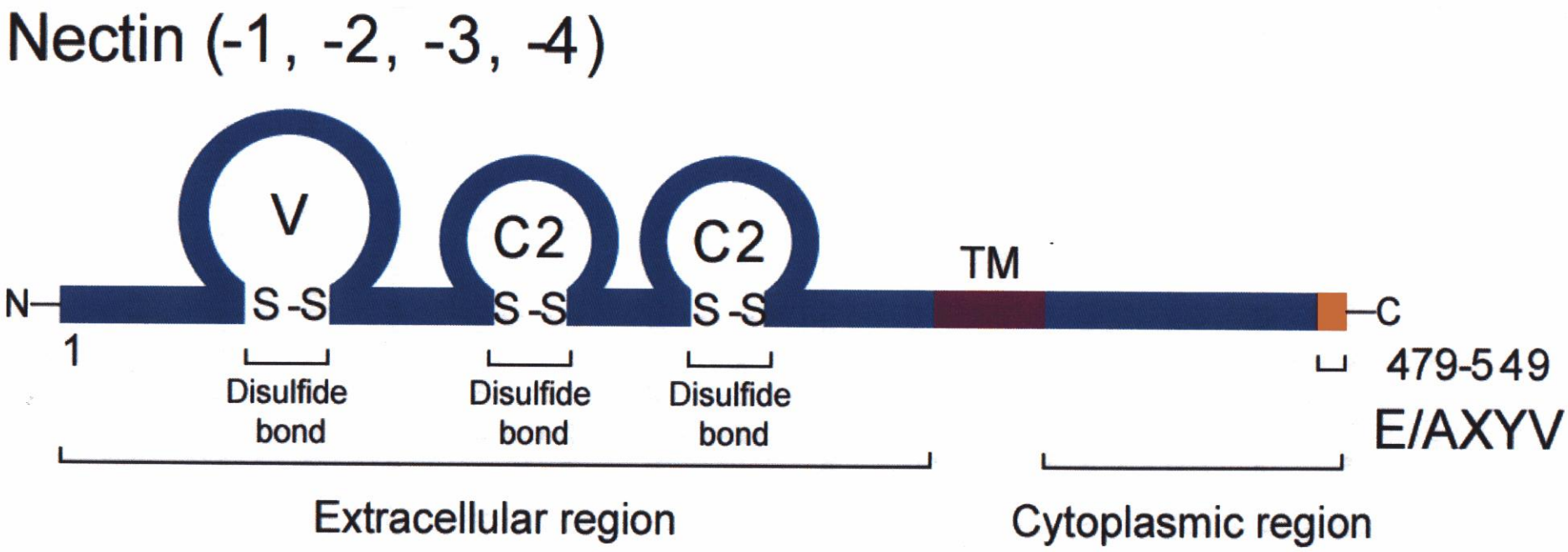

Figure 5 Molecular structure of nectin

Nectins, which comprise a family of at least four members, nectin-1, -2, -3 and nectin-4, has an extracellular region containing three tandemly aligned Ig-like domains (V, C2, C2) with disulfide bonds (S-S), a single transmembrane region (TM) and a cytoplasmic region. The cytoplasmic region contains a conserved motif of four amino acid residues (E/AXYV) at their carboxyl termini (-C), and this binds the PDZ domain of afadin (**see Figure 1**). N- represents anino termini.

1.4. Aim

Combining cadherin and nectin data has led to a "fork initiation and zipper" hypothesis for the formation of cell-cell adhesions, whereby nectins initiate cell-cell adhesions followed by the recruitment of cadherins and the formation of AJs (**Figure 6**)(Irie, Shimizu et al. 2004). In order to test this hypothesis, however, further detail regarding the molecular basis of the mechanical interactions involving extracellular multiple domains for both nectins and cadherins need to be investigated. We here address this issue. Recent progress in single-molecule force measurement methods, so-called dynamic force spectroscopy (DFS), has allowed us to probe the inner world of complex molecular interactions that are difficult or impossible to detect in assays near equilibrium but that determine the characteristics of the interactions(Evans 2001). Making it the preferred tool to detect weak interaction forces between biomolecules(Kishino and Yanagida 1988; Ishijima, Doi et al. 1991; Kitamura, Tokunaga et al. 1999), our IFM force measurement system has improved force resolution to the sub-piconewton level with a response time of sub-millisecond level by using a flexible glass microneedle(Tokunaga, Aoki et al. 1997), an approximately several tens-fold higher force sensitivity than

conventional atomic force microscopy (AFM)(Marshall, Long et al. 2003). We extended this technique to the molecular interactions involving multiple domain structures between paired CAMs. Three different bound states between paired nectins and four different bound states between paired cadherins were directly identified based on bond strength distribution, and the dynamic properties of these states were characterized. The results indicate that multiple tandem aligned domains of nectins act uncooperatively, as a zipper-like multiply bonded system while those of cadherins act cooperatively, as a parallel multiply bonded system. We discuss our results based on a "fork initiation and zipper" hypothesis for the formation of cell-cell adhesion (**Figure 6**)(Irie, Shimizu et al. 2004).

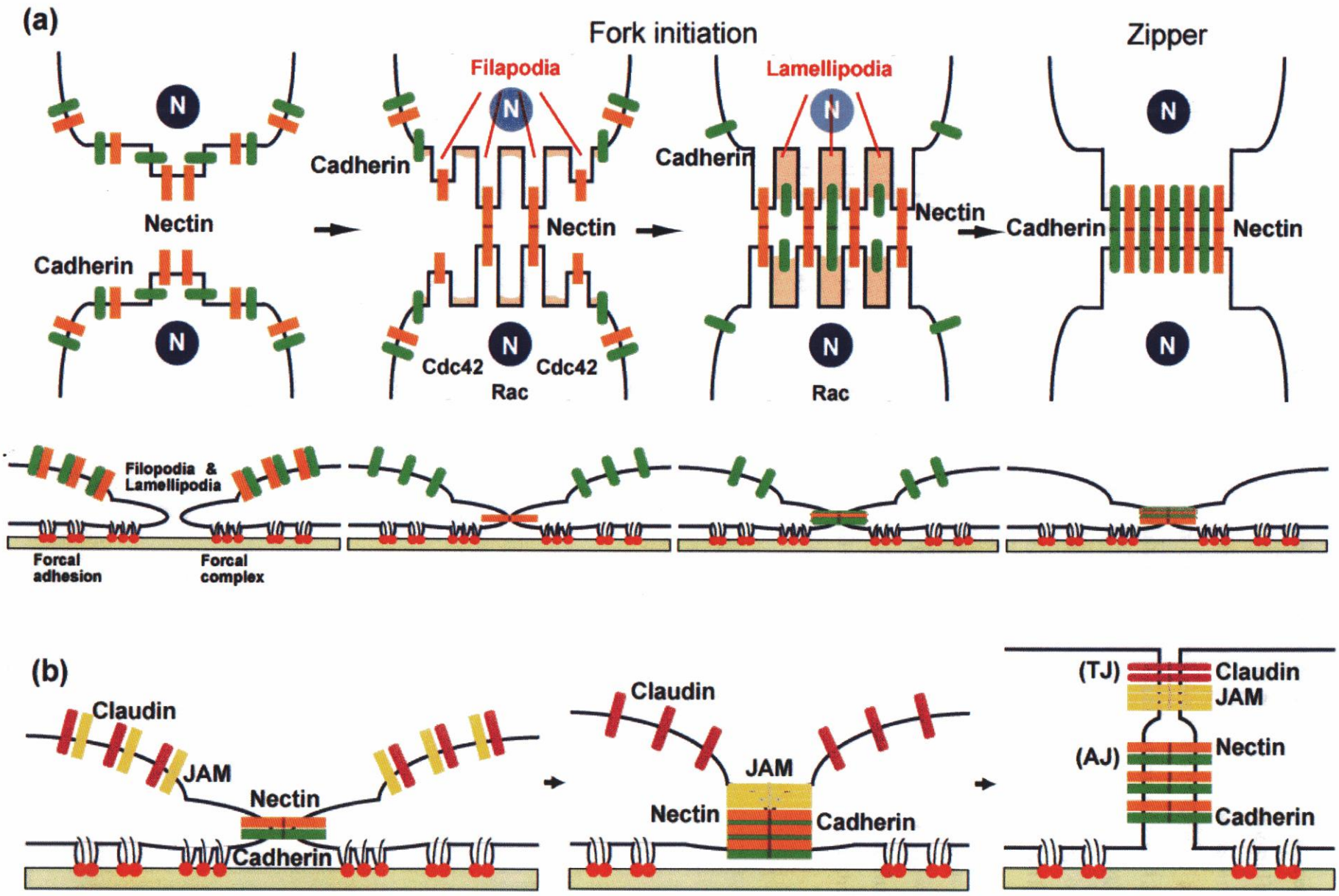
(a)
Fork initiation
Zipper
Filapodia
Lamellipodia
N
Nectin
Cadherin
Cdc42
Rac
Filopodia &
Lamellipodia
Forcal
adhesion
Forcal
complex
(b)
Claudin
JAM
Nectin
Cadherin
(TJ)
(AJ)

Figure 6 Fork initiation and zipper hypothesis

(**a**) Formation of AJs. Nectins and E-cadherin are diffusely distributed on the free surface of the plasma membrane of migrating cells. When the two migrating cells contact through their protrusions, nectin form *trans*-dimers that form microclusters at intercellular contact sites. The nectin-based microclusters are mainly formed at the initial stage. The *trans*-interactions of nectins induce the activation of Cdc42, resulting in increase in the number of filopodia and cell–cell contact sites like "Fork initiation". GTP-Rac formed by either the *trans*-interactions of nectins or that of E-cadherin induces formation of lamellipodia. The lamellipodia efficiently expand the cell–cell adhesion between the filopodia, and efficiently zip the cell–cell contact sites, so called "Zipper". Nectins- and E-cadherin-based AJs are formed. Upper panel, transverse section view; lower panel, cross-section view. (**b**) Formation of TJs. During the formation of AJs, JAM is first assembled at the apical side, followed by the recruitment of claudin, which eventually leads to the establishment of TJs (cross-section view).

2. Single molecule bond strength measurement system

2.1. Proteins

Nectin-1-Fc (Nef-1), nectin-3-Fc (Nef-3) and E-cadherin-Fc (Cef) fusion proteins were generated by placing the respective cDNA fragment coding for the complete extracellular portion of nectin-1, nectin-3 and E-cadherin in front of a cDNA fragment coding for the Fc portion of human IgG for homo-*cis*-dimerising (**Figure 7**). Construction of the expression plasmid, cell transfection, and production of the fusion protein was done as previously described(Honda, Shimizu et al. 2003). The secreted Cef, Nef-1 and Nef-3 fusion proteins were purified from High Five insect cells (Invitrogen, USA) by affinity chromatography using protein A-Sepharose beads (GE healthcare, USA). The purified proteins were frozen and stored at –80 °C until use.

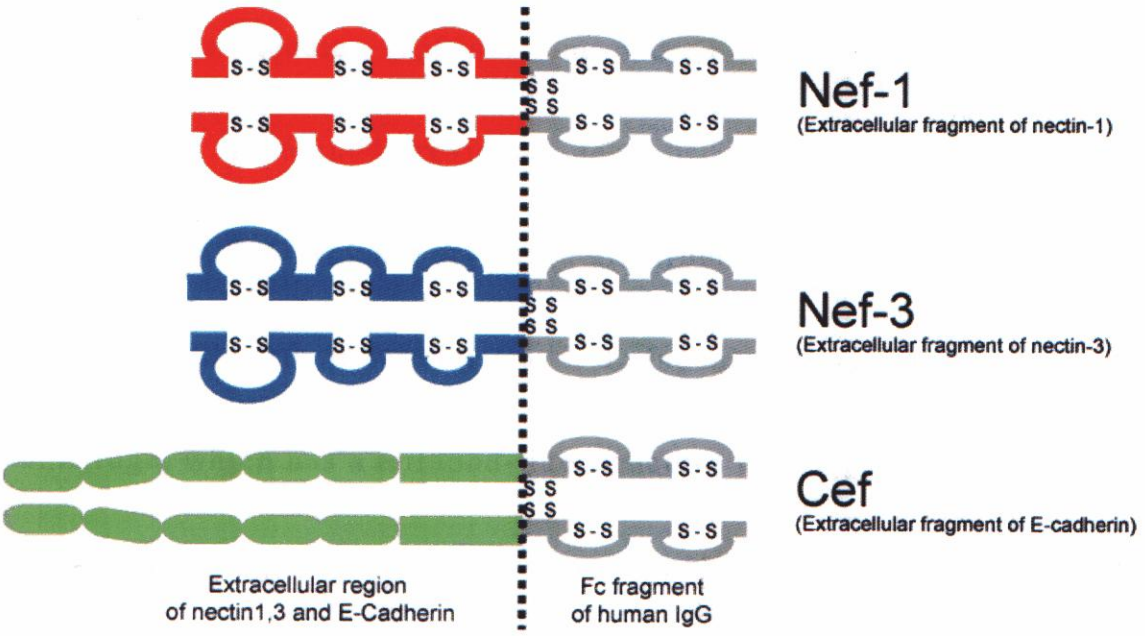

Figure 7 Protein construction

The extracellular region of nectin-1, nectin-3 and E-cadherin is fused to Fc fragment of human IgG. Nef-1, Nef-3 and Cef represent the extracellular fragment of nectin-1, nectin-3 and E-cadherin, respectively. S-S represents the disulfide bonds.

2.2. Scanning probe and plate

The scanning probe consisted of a thin glass needle and a ZnO whisker crystal. The thin glass needle, ~150 μm long and <1 μm in diameter, was prepared according to the method previously described (**Figure 8**)(Ishijima, Kojima et al. 1996). A ZnO whisker crystal (a gift from Central Research Laboratories, Matsushita Electric Industrial Co, Ltd, Japan) cutting one of the legs by a centrifuge, which has a tetrapod-like structure with legs typically of 5–10 μm in length and a tip radius of ~15 nm, was used as the tip of the scanning probe. The ZnO whisker crystal was attached to the tip of the glass needle with epoxy resin with one of the legs pointed downward using a micromanipulator under a binocular microscope. Glass microbead (Bangs Laboratories, USA) probes of diameter 1.50 μm or 3.28 μm and plates of diameter 3.28 μm or 5.06 μm were amino-silanized in 5 % (v/v) aminosilane (Shin-Etsu Chemical, Japan) in water overnight at room temperature. The glass microbeads were modified covalently by a polyethylene glycol (PEG) spacer containing an amino-reactive crosslinker group (*N*-hydroxysuccinimide ester, NHS ester) at one end (Shearwater Polymers, USA) in CH_3Cl containing 3 μM PEG and 0.5 % triethylamine overnight at room temperature. The mixture was washed

several times with and stored in CH_3Cl. Then, the glass microbead probes were glued to the tip of the ZnO whisker with epoxy resin under a binocular microscope (**Figure 8**)(Tokunaga, Aoki et al. 1997).

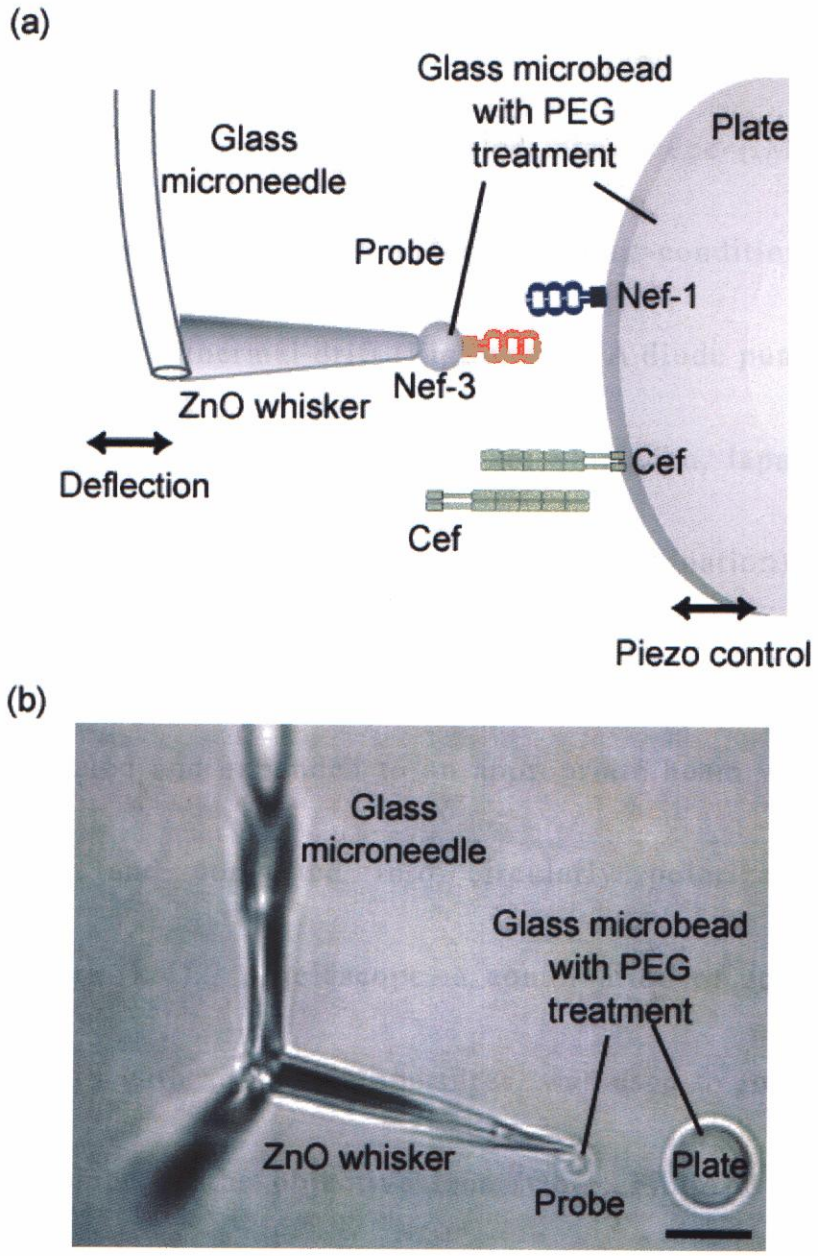

Figure 8 Bond strength measurement system

(**a**) Schematic drawing of bond strength measurements. The probe consists of a flexible glass microneedle and a ZnO-whisker-glassmicrobead. The deflection data of the probe in the direction of the arrow were acquired from a split photodiode (**left**). The glass microbead plate attached to a coverslip was controlled by the piezo stage with sub-nanometer accuracy in the direction of the arrow (**right**). Nectin-1 chimera protein (Nef-1), nectin-3 chimera protein (Nef-3) and E-cadherin chimera protein (Cef) were immobilized to the glass microbead probe and plate with PEG treatment. (**b**) Bright field image of bond strength measurements. Scale bar, 5 μm.

2.3. Microscope apparatus

The setup of IFM was based on an inverted microscope (IMT-2; Olympus, Japan), sitting on an air table in a soundproof and air-conditioned chamber to minimize vibration and thermal drift (**Figure 9**). A diode pumped frequency doubled Nd: YAG laser (λ=532 nm; HK-5526; Shimadzu, Japan) was used as the light source for nanometry (transmitted light illumination). A divergent and linearly polarized beam from the laser through a neural density filter (ND) was collimated and expanded to an appropriate beam width by a beam expander (Exp), and converted into circularly polarized beam by a quarter-wave plate (λ/4). A telescope, a combination of concave (L1) and convex (L2) lenses with adjustable apertures, was used to focus the beam at the back focal plane of the objective lens (Obj1; PlanApo 100X 1.40 oil; Olympus, Japan), achieving Köellar illumination. The size of the field of view was adjusted to ~30 μm in diameter by changing the size of the aperture. The laser power at the nosepiece was ~5 mW. The green lasers were introduced into the objective lens (Obj1) using a dichroic mirror (DM1; FF545/650-D101; Semrock, USA). The bright field image by Kr lamp (MB-48PF5K/2B; Matsushita Electric Industrial Co, Ltd, Japan) illumination

through bandpass filter (BF; Olympus, Japan) and a dichroic mirror (DM2; FF545/650-D101; Semrock, USA) was collected by Obj1 and passed through the dichroic mirror (DM1). Background fluorescence and scattered incident laser light were rejected by a holographic notch filter (NF; HNPF-532AR-1.0; Kaiser Optical Systems Inc., USA) and an interference bandpass filter (BF; FF562-Em02-25; Semrock, USA). The bright field image was magnified by a projection lens (PL; PE5; Olympus, Japan) and detected by an intensified SIT camera (ISIT), which consists of an image intensifier (VS4-1845; Video Scope International Ltd., USA) and an SIT camera (C2400- 08; Hamamatsu Photonics, Japan). The bright field image of the probe was formed by a long working distance objective lens (Obj2; Plan 60 DIC/LWD; Nikon, Japan), introduced using a dichroic mirror (DM2) and magnified by a concave lens (L3) to the final magnification of ~300×. The magnified image of the probe was projected onto a split-photodiode (PD; S2721-02; Hamamatsu Photonics, Japan).

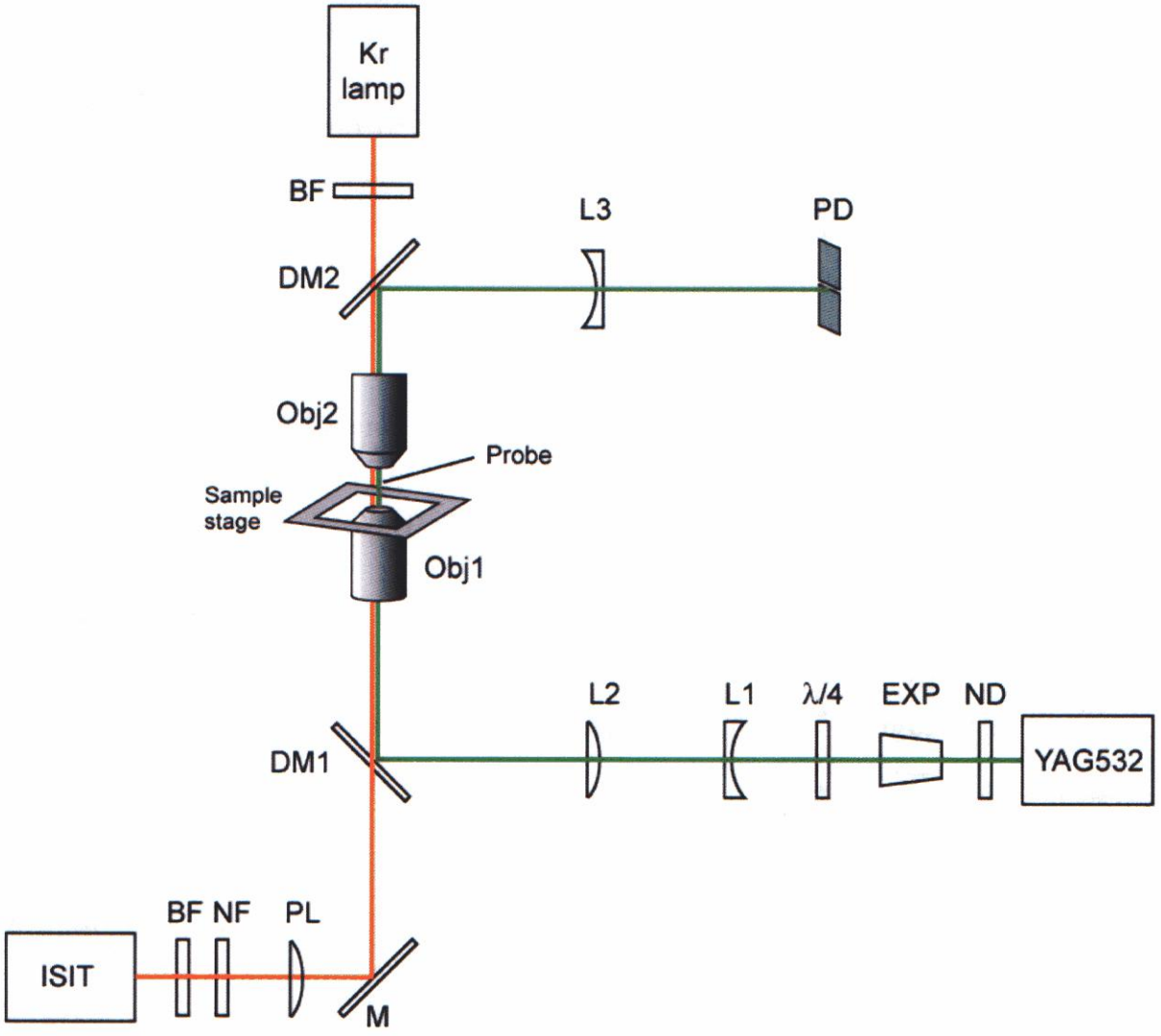

Figure 9 Schematics of the microscope apparatus

The system was built on an inverted microscope. A green laser (YAG532) was used as the light source for nanometry (transmitted light illumination). The bright field image by Kr lamp illimination was collected by the lower objective (Obj1), magnified by a projection lens (PL), and detected by an intensified-SIT camera (ISIT). The magnified image of the probe was obtained by the upper objective (Obj2) and a concave lens (L3). Displacement of the needle was monitored using a split-photodiode (PD). ND, neutral density filter; Exp, beam expander; λ/4, quarter-wave plate; L1&3, concave lenses; L2, convex lens; DM1&2, dichroic mirrors; NF, notch filter; BF, bandpass filters; and M, mirrors.

2.4. Performance of the apparatus

Figure 10a and **b**, shows the differential output signals when sinusoidal displacements with amplitudes of 0.1 and 1 nm were applied to the stiff needle attached to the stage, respectively. The output signals were recorded with a bandwidth of 24 kHz. The traces are shown single runs with passing them through a low-pass filter. Thus, the displacement of 0.1 nm could be clearly observed. The thermal vibrations of the needle were small because of its very high stiffness. **Figure 10c** shows the relationship between the displacements and the differential outputs when the stage with a pair of photodiodes was moved with constant velocity. The outputs were linearly proportional to applied displacements in the wide range from 0 to approximately 700 nm.

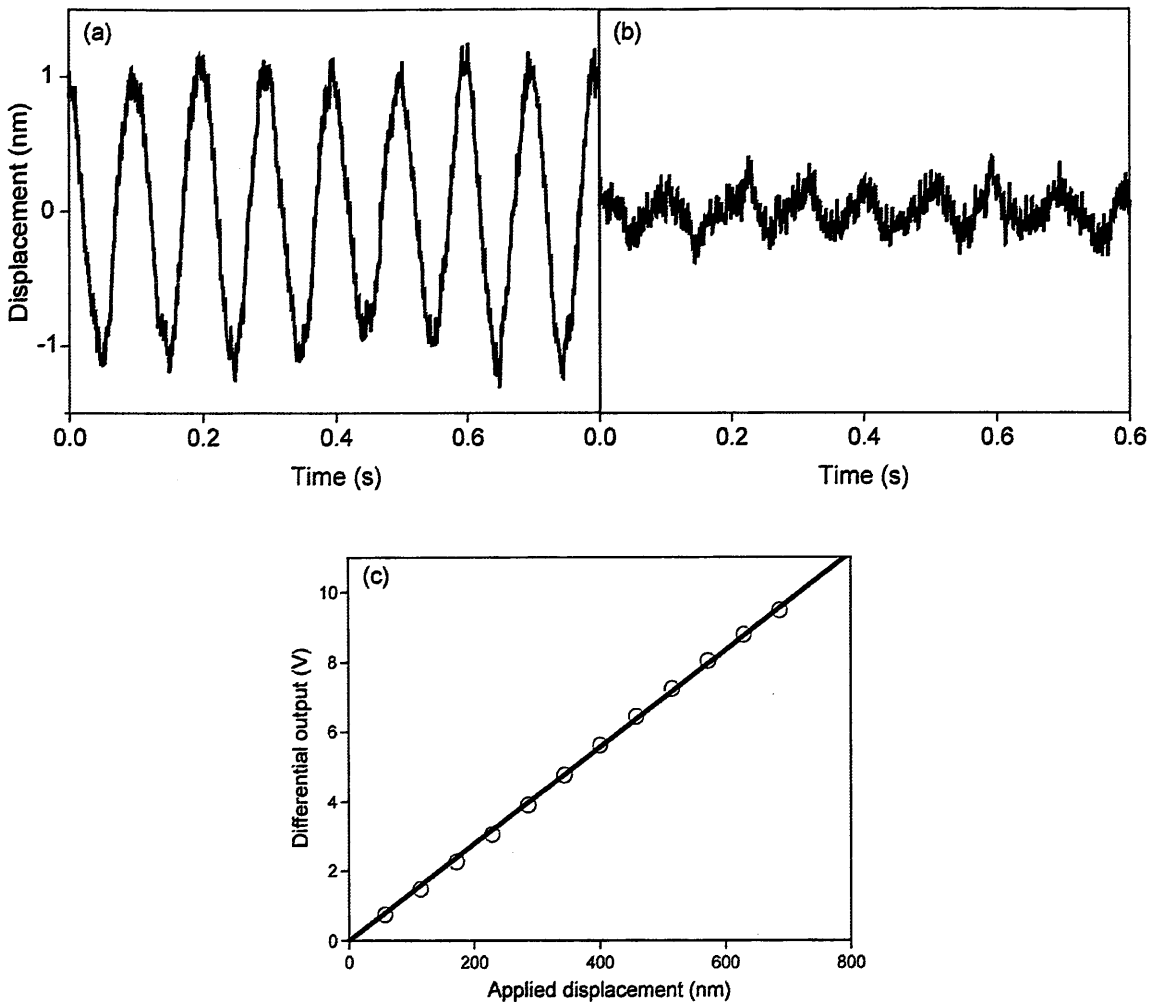

Figure 10 Spatial resolution and linearity of differential outputs

(**a** and **b**) Changes in the differential outputs from a pair of photodiodes when sinusoidal length changes were applied to the ZnO whisker attached to the stage with amplitudes of 1 nm (**a**) and 0.1 nm (**b**). The signals were recorded with a 24-kHz band width. Traces show single runs with passing them through a low-pass filter. (**c**) Relationship between displacements and differential outputs. Plots show the changes in the differential output when the stage with a pair of photodiodes was moved with constant velocity.

2.5. Single molecule bond strength measurements

2.5.1. Experimental preparation

The plates were washed several times with phosphate-buffered saline (140 mM NaCl, 1.5 mM KH_2PO_4, 8.1 mM $Na_2HPO_4 \cdot 12H_2O$ 2.7 mM KCl, adjusted with NaOH to pH = 7.4) and mixed with Cef or Nef-1 solution at a concentration of approximately 500 molecules/μm^2 surface. The protein-coated plates were stored at 4 ℃ until use. A solution containing the protein-coated plates was applied to a coverslip. Unbound protein-coated plates were washed out with assay buffer (140 mM NaCl, 1.5 mM KH_2PO_4, 8.1 mM $Na_2HPO_4 \cdot 12H_2O$ 2.7 mM KCl, adjusted with NaOH to pH = 7.4 in Nef-Nef experiments; 50 mM NaCl, 1 mM $CaCl_2$, 20 mM Hepes, adjusted with NaOH to pH = 7.35 in Cef-Cef experiments). The probe was positioned above a second chamber of the coverslip, washed with assay buffer and mixed with Cef or Nef-3 solution at a variety of concentrations for 15-30 min before bond strength measurements.

2.5.2. Bond strength measurement system

Bond strength measurements between paired CAMs were conducted by approach-retrace cycles of the plate to the probe at a variety of amplitudes and frequencies, in the range of 10-10^4 pN/s, with approximately constant contact time at each loading rate and approximately constant maximum contact force at a variety of loading rates (**Figure 8**). The spring constant of the glass microneedle was 0.01-1 pN/nm determined by thermal fluctuation analysis or cross calibration method(Ishijima, Kojima et al. 1996). The nominal loading rate, Kv, was pre-selected by setting the spring constant, K, and piezo speed, v, in the range of 100-10,000 nm/s, and determined before bond strength measurements. The period following detachment was used to determine the mean value of the deflection of the probe (neutral position). Bond strength values of detachment events were calculated using the distance from the neutral position and the spring constant of the glass microneedle. The deflection data of the probe with sub-nanometer resolution was measured as the differential output of the photodiode with the magnified image of the probe projected (**Figure 11**). The photocurrents of the photodiodes were amplified and converted into a voltage signal and the difference was

calculated by a custom-made amplifier system (Amp.; Sentech, Japan). The output signal was acquired for online monitoring and recording at 10 kHz with 16 bits resolution by a PC with a DAQ board as a D/A converter (PCI-MIO-16XE-10; National Instruments Co., USA) using a LabVIEW software (National Instruments) based custom program(Kitamura, Tokunaga et al. 2005). They were analyzed with LabVIEW software (National Instruments) based custom program and Origin software (Microcal).

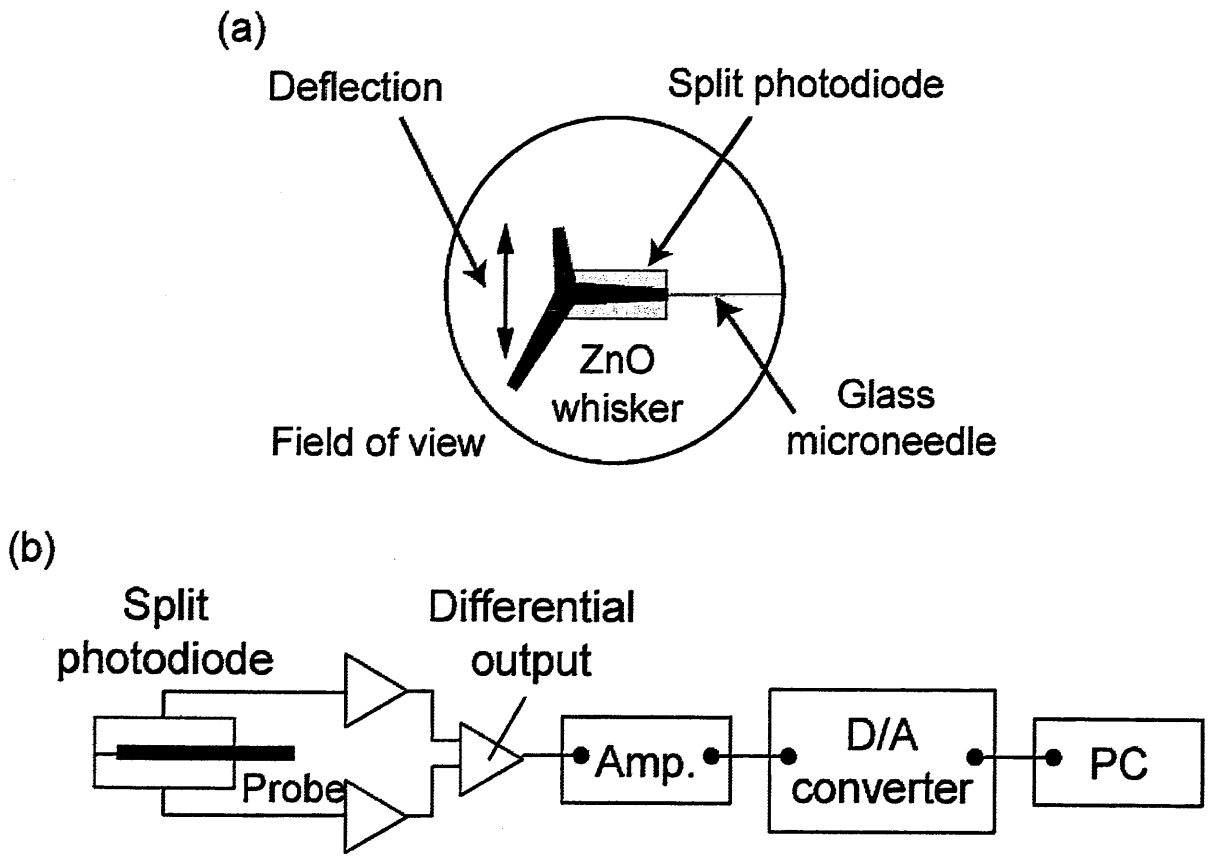

Figure 11 Data acquisition system

(a) The schematics of the measurement geometry. A ZnO whisker crystal, whose length was 5–10 μm and radius of curvature of the tip was ~15 nm, was attached to the tip of a very fine glass microneedle, ~150 μm long and <1 μm in diameter. The magnified image of the whisker + needle was projected onto the split-photodiode to measure the nanometer deflection. (b) The schematics of the data acquisition system. The deflection data of the probe was measured as the differential output of the photodiode with the magnified image of the probe. The photocurrents of the photodiodes were amplified and converted into a voltage signal and the difference was calculated by a custom-made amplifier system (Amp.). The output signal was acquired for online monitoring and recording by a PC with a D/A converter.

2.6. Potential of IFM system for high sensitive force measurement

2.6.1. High sensitive force measurement

Our IFM system has improved force resolution to the sub-piconewton level with a response time at the sub-millisecond level by using a flexible glass microneedle(Tokunaga, Aoki et al. 1997), a significant improvement over other force measurement systems such as AFM(Binnig, Quate et al. 1986) and biomembrane force probe (BFP)(Evans, Ritchie et al. 1995), making it the preferred tool to detect weak interaction forces between biomolecules(Kishino and Yanagida 1988; Ishijima, Doi et al. 1991; Kitamura, Tokunaga et al. 1999). The force sensitivity of the IFM system can be described as follows. A force, F, deflects a cantilever with stiffness, K. The displacement, x, caused by F is given by

$$x = \frac{F}{K}.$$

According to the equipartition principle, the thermal fluctuations of a glass microneedle, Δx, are given by

$$\sqrt{\langle \Delta x^2 \rangle} = \sqrt{\frac{k_B T}{K}}.$$

If the system noise is due solely to thermal bending motions, the

signal-to-noise ratio is then

$$\frac{\left(\frac{F}{K}\right)}{\sqrt{\frac{k_B T}{K}}} = \frac{\left(\frac{F}{\sqrt{k_B T}}\right)}{\sqrt{K}}.$$

For example, when a force of 0.5 pN is measured by a glass microneedle with a spring constant of 0.01 pN/nm, the signal to noise ratio is >2.4, which is approximately 30-fold higher than conventional AFM using a cantilever with a spring constant of 10 pN/nm (Tokunaga, Aoki et al. 1997).

2.6.2. High sensitive bond strength measurement

Using our IFM system we measured the force applied to the interaction between paired CAMs at the detachment event during approach-retrace cycles of the plate to the probe (**Figure 8** and **see Chapter 2**). **Figure 12a** shows a typical time course for single detachments, defined as single step detachments following linear increments of force applied to the interaction, between paired CAMs during approach-retrace cycles. Actually, Sub-piconewton forces between paired CAMs were clearly resolved. When the interaction probability was less than 0.35, most detachments (>99 %) were observed as single detachment. When the interaction probability was larger than 0.5, multiple detachments, defined as multiple step detachments following linear increments of force applied to the interaction, were observed (**Figure 12b**). Few interactions were observed in the control experiments where no proteins or BSA were present, indicating that the observed events were not due to non-specific attachments between the plate and the probe (**Figure 12c**).

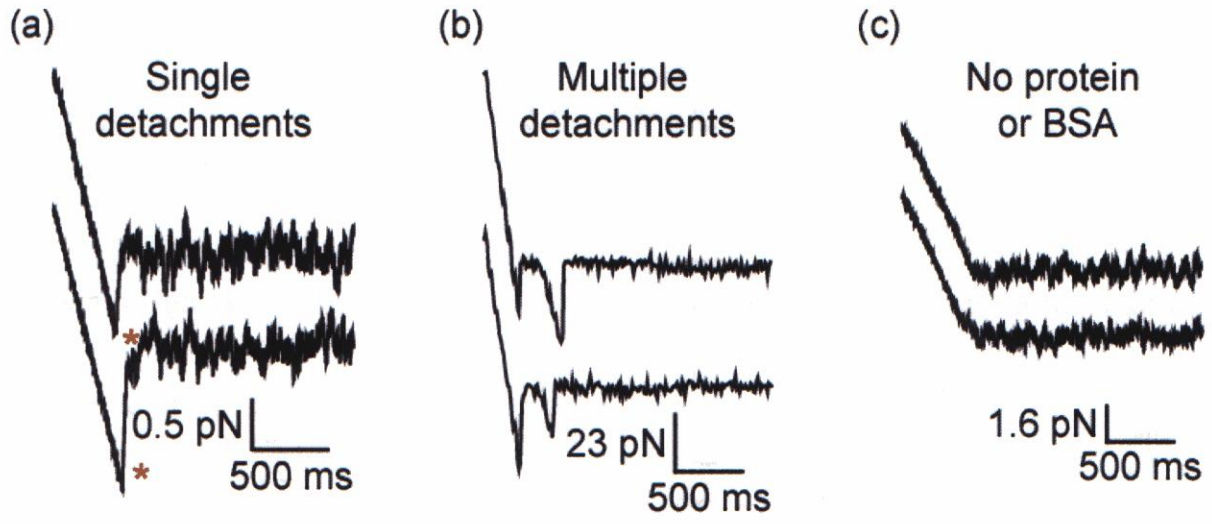

Figure 12 Bond strength measurement system

(**a** - **c**) Typical time courses of the force applied to the interaction between paired CAMs during approach-retrace cycles of the plate to the probe. Asterisks in (**a**) mark detachment events taken for bond strength values. Detachment events were specifically observed between paired CAMs (**a** for single detachments and **b** for multiple detachments) but not in the absence of proteins or in the presence of BSA (**c**). Here, the interactions between paired nectins are shown.

3. Theory for bond strength analysis

3.1. Thermal activation model

Based on thermal activation model as developed by Kramers (**Figure 13a**)(Kramers 1940), the dissociation rate, $k(f)$, of a molecular bond in the presence of an applied external force, f, is written as

$$k(f)=\left(\frac{1}{\tau_D}\right)\exp\left(\frac{-(E-fd)}{k_BT}\right)$$

, where τ_D is the diffusive relaxation time, E is the barrier energy for the dissociation, k_B is Boltzman's constant, T is the absolute temperature and d is the bond length.

Consequently, the dissociation rate under an external force is related to the lifetime in the absence of applied external force, τ_0, according to

$$k(f)=\left(\frac{1}{\tau_0}\right)\exp\left(\frac{f}{f_T}\right)$$

, where

$$\tau_0=\tau_D\exp\left(\frac{E}{k_BT}\right)$$

and

$$f_T=\frac{k_BT}{d}.$$

Thus, when a molecular bond is subjected to an external force, the dissociation rate increases exponentially with force as first postulated by

Bell(Bell 1978).

Under a steady ramp of force, i.e.

$$f = r^* t$$

, where r^* is the loading rate, the dissociation rate increases exponentially with time, t, and a first-order Markov equation predicts that the likelihood of bond survival to a particular time, $S(t)$, will fall rapidly, according to

$$S(t) = \exp\left(-\int_{0\to t} k(r^* t')dt'\right)$$

, in the absence of rebinding.

Recognizing that the time course of bond survival is equivalent to the rising force, the likelihood of bond survival to a particular force, $S(f)$, is found by a simple transformation to be a function of the loading rate, i.e.

$$S(f) = \exp\left(\left(-\frac{f_T}{r^* \tau_0}\right)\left(\exp\left(\frac{f}{f_T}\right)-1\right)\right).$$

The bond strength probability density for a particular loading rate, $p(f)$, is specified by multiplying the likelihood of bond survival with the dissociation rate and normalizing as

$$p(f) = \left(\frac{1}{r^* \tau_0}\right)\exp\left(\frac{f}{f_T}\right)\exp\left(\left(-\frac{f_T}{r^* \tau_0}\right)\left(\exp\left(\frac{f}{f_T}\right)-1\right)\right)$$

, where the bond strength, f, is defined as the force necessary to break a bond

(**Figure 13b**)(Evans and Ritchie 1997).

Using this bond strength distribution, the most frequent force, f^*, can be described as

$$f^* = f_T \ln\left(\frac{\tau_0}{f_T}\right) + f_T \ln(r^*)$$

by solving

$$\frac{\partial p(f)}{\partial f} = 0$$

(**Figure 14**),

and the standard deviation, σ, can be characterized as

$$\sigma \approx 1.2\left(\frac{k_B T}{d}\right)$$

(**Figure 15**)(Perret, Leung et al. 2004).

On a the most frequent force-loading rate plotting, the slope, f_T, is related only to d,

$$f_T = \frac{k_B T}{d}$$

, while the intercept, f^*_0, is related to τ_0 and f_T

$$f^*_0 = f_T \ln\left(\frac{f_T}{\tau_0}\right)$$

(**Figure 16**).

Complex molecular bonds such as macromolecular zippers(Merkel, Nassoy et al. 1999; Evans, Leung et al. 2001) can create a mountainous terrain of barrier

energies(Evans 2001). The dissociation rate is governed by the sum of the times needed to transit the individual barrier energy, i.e.

$$k(f)=\left(\sum \tau_0(n)\exp\left(\frac{-f}{f_T(n)}\right)\right)^{-1}$$

, where $\tau_0(n)$ is the lifetime in the absence of applied external force for the nth barrier energy and $f_T(n)$ is the thermal force for the nth barrier energy,

$$f_T(n)=\left(\frac{k_BT}{d(n)}\right)$$

,where $d(n)$ is the bond length for the nth barrier energy(Evans, Leung et al. 2001).

Under the steady ramp of force, the most frequent force of the bond strength distribution can be related to loading rate, according to

$$\frac{1}{r^*}=\sum\left(\left(\frac{\tau_0(n)}{f_T(n)}\right)\exp\left(\frac{-f^*}{f_T(n)}\right)\right)$$

(Evans, Leung et al. 2001).

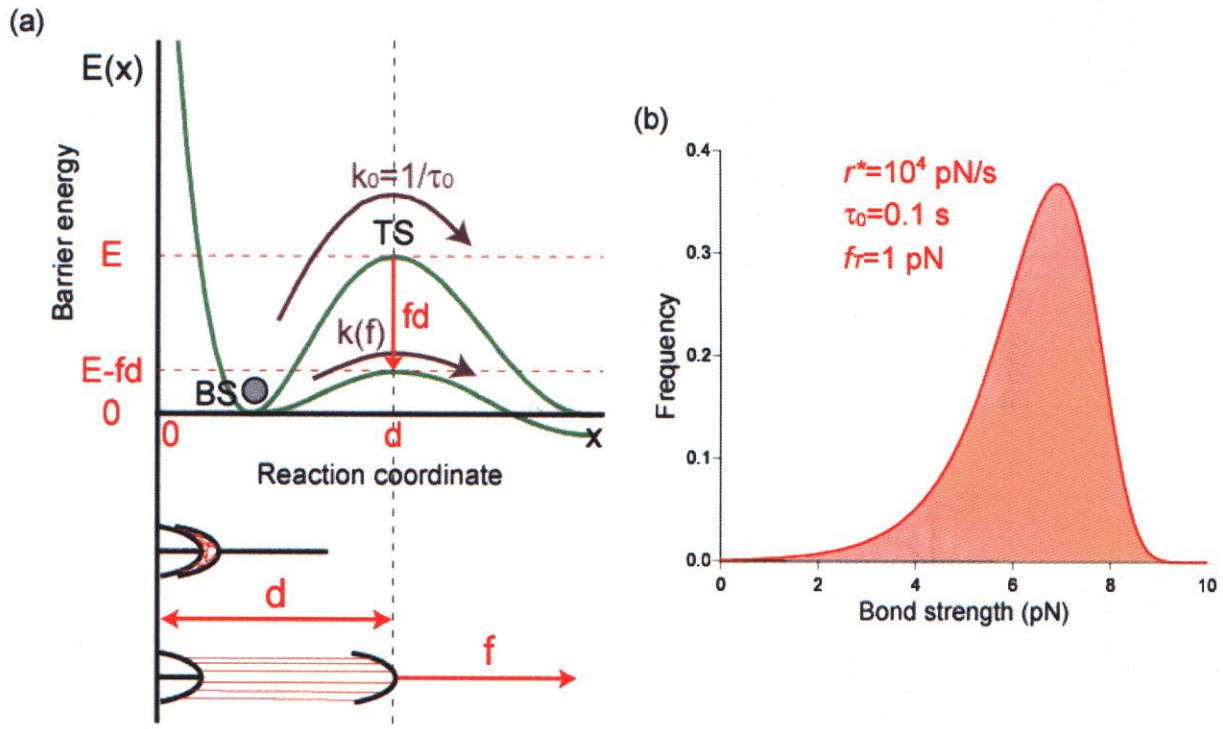

Figure 13 Thermal activation model

(**a**) Conceptual energy landscape for molecular bonds. The dissociation rate in the absence of applied force, f, is written by diffusive relaxation time, τ_D, and the thermal likelihood of reaching the top of barrier energy, $\exp(-E/k_BT)$, as $k_0 = 1/\tau_0 = (1/\tau_D)\exp(-E/k_BT)$, where k_0 is the dissociation rate in the absence of applied force, τ_0 is the lifetime in the absence of the applied force, E is the barrier energy for the dissociation, k_B is Boltzman's constant and T is the absolute temperature. The barrier energy is lowered by applied force in proportion to the distance between bound state (BS) and transition state (TS) along the reaction coordinate, d, which can be interpreted as bond length of molecular bonds (lower), i.e. $-fd$, assuming that the location of the TS is insensitive to force. Thus, the dissociation rate in the presence of applied force, $k(f)$, is written as $k(f) = (1/\tau_D)\exp(-(E - fd)/k_BT)$. (**b**) Theoretical bond strength distribution under a steady ramp of applied force. Red distribution was calculated by bond strength probability density function, $p(f) = (1/(r^*\tau_0))\exp(f/f_T)\exp(-(f_T/(r^*\tau_0))(\exp(f/f_T) - 1))$, with $r^* = 10^4$ pN/s, $\tau_0 = 0.1$ s and $f_T = 1$ pN, where r^* is the loading rate, f_T ($= k_BT/d$) is the thermal force.

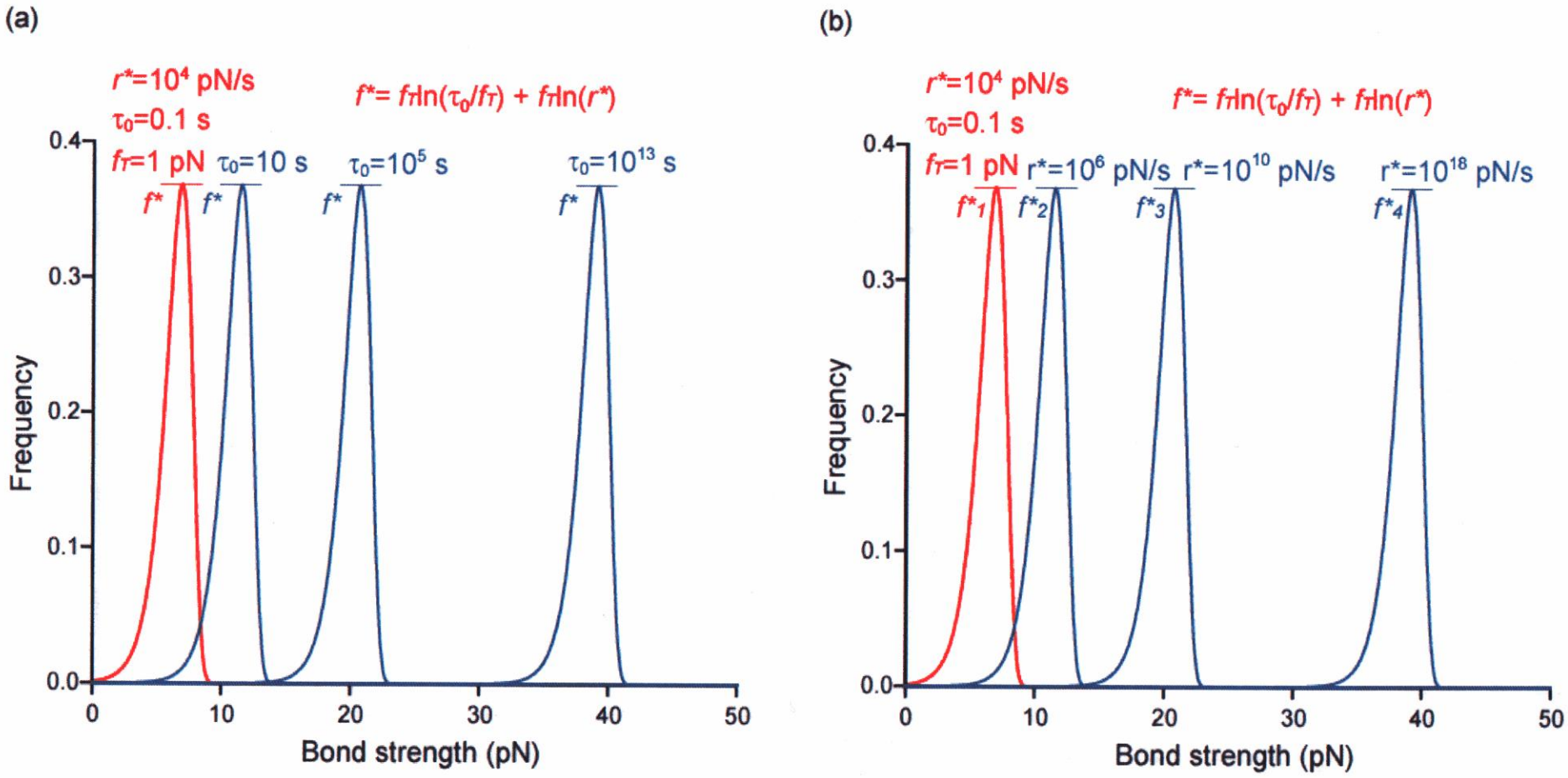
(a)
r*=10^4 pN/s
τ0=0.1 s
fT=1 pN
f*= fTln(τ0/fT) + fTln(r*)
τ0=10 s
τ0=10^5 s
τ0=10^13 s
f*
f*
f*
f*
Frequency
0.0
0.1
0.2
0.3
0.4
0
10
20
30
40
50
Bond strength (pN)
(b)
r*=10^4 pN/s
τ0=0.1 s
fT=1 pN
f*= fTln(τ0/fT) + fTln(r*)
r*=10^6 pN/s
r*=10^10 pN/s
r*=10^18 pN/s
f*1
f*2
f*3
f*4
Frequency
0.0
0.1
0.2
0.3
0.4
0
10
20
30
40
50
Bond strength (pN)

Figure 14 The most frequent force on bond strength distribution

(**a**) Lifetime dependency of the most frequent force. Red distribution represents bond strength probability density function, $p(f)$, with $r^* = 10^4$ pN/s, $\tau_0 = 0.1$ s and $f_T = 1$ pN, similar to **Figure 13b**. Blue distributions represent bond strength probability density functions, $p(f)$, at $\tau_0 = 10$ s, 10^5 s and 10^{13} s, respectively, with $r^* = 10^4$ pN/s and $f_T = 1$ pN. (**b**) Loading rate dependency of the most frequent force. Red distribution represents bond strength probability density function, $p(f)$, at $r^* = 10^4$ pN/s, $\tau_0 = 0.1$ s and $f_T = 1$ pN, similar to **Figure 13b**. Blue distributions represent bond strength probability density functions, $p(f)$, at $r^* = 10^6$ pN/s, 10^{10} pN/s s and 10^{18} pN/s, respectively, with $\tau_0 = 0.1$ s and $f_T = 1$ pN. The most frequent force on bond strength distribution is written by solving $\partial p(f)/\partial f = 0$ as $f^* = f_T \ln(\tau_0 / f_T) + f_T \ln(r^*)$. f^*, f^*_1, f^*_2, f^*_3 and f^*_4 represent the most frequent force of bond strength distributions, respectively.

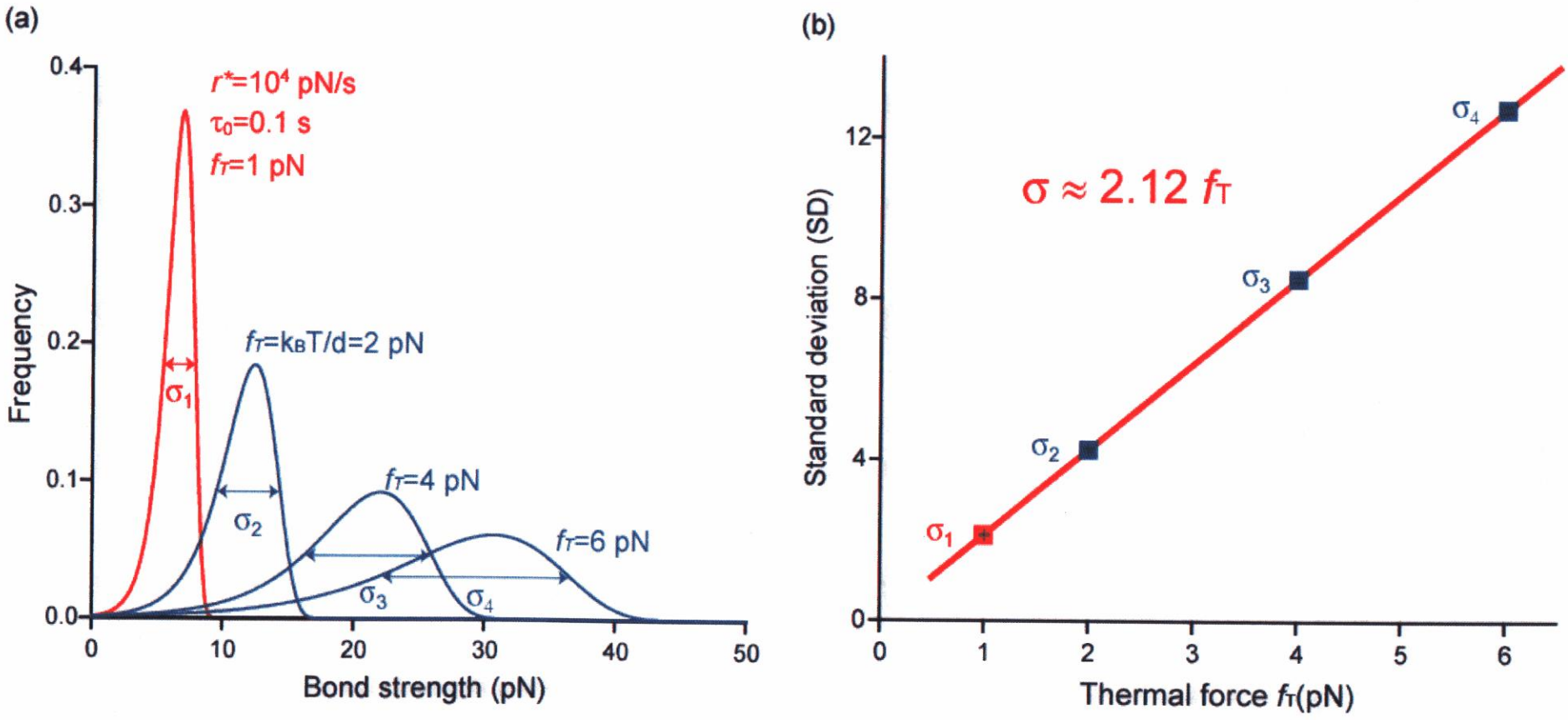
(a)
r*=10⁴ pN/s
τ₀=0.1 s
fT=1 pN
fT=kBT/d=2 pN
fT=4 pN
fT=6 pN
σ1
σ2
σ3
σ4
Frequency
Bond strength (pN)
0.0
0.1
0.2
0.3
0.4
0
10
20
30
40
50
(b)
σ ≈ 2.12 fT
Standard deviation (SD)
Thermal force fT(pN)
0
4
8
12
0
1
2
3
4
5
6

Figure 15 Thermal force on bond strength distribution

Thermal force dependency of the bond strength distribution. Red distribution represents bond strength probability density function, $p(f)$ at $r^* = 10^4$ pN/s, $\tau_0 = 0.1$ s and $f_T = 1$ pN. Blue distributions represent bond strength probability density functions, $p(f)$, at $f_T = 1$ pN, 2 pN, 4 pN and 6 pN respectively, with $\tau_0 = 0.1$ and $r^* = 10^4$ pN/s. Standard deviations (SD) of bond strength distributions, σ_1, σ_2, σ_3 and σ_4, respectively, were estimated by Gaussian approximation. (**b**) The relationship between thermal force and standard deviation (SD). Standard deviations (SD) of bond strength distributions were plotted against thermal force, f_T. The standard deviation (SD) of bond strength distribution is characterized as a function of d, $\sigma \approx 2.12 f_T$, where $f_T = k_B T / d$.

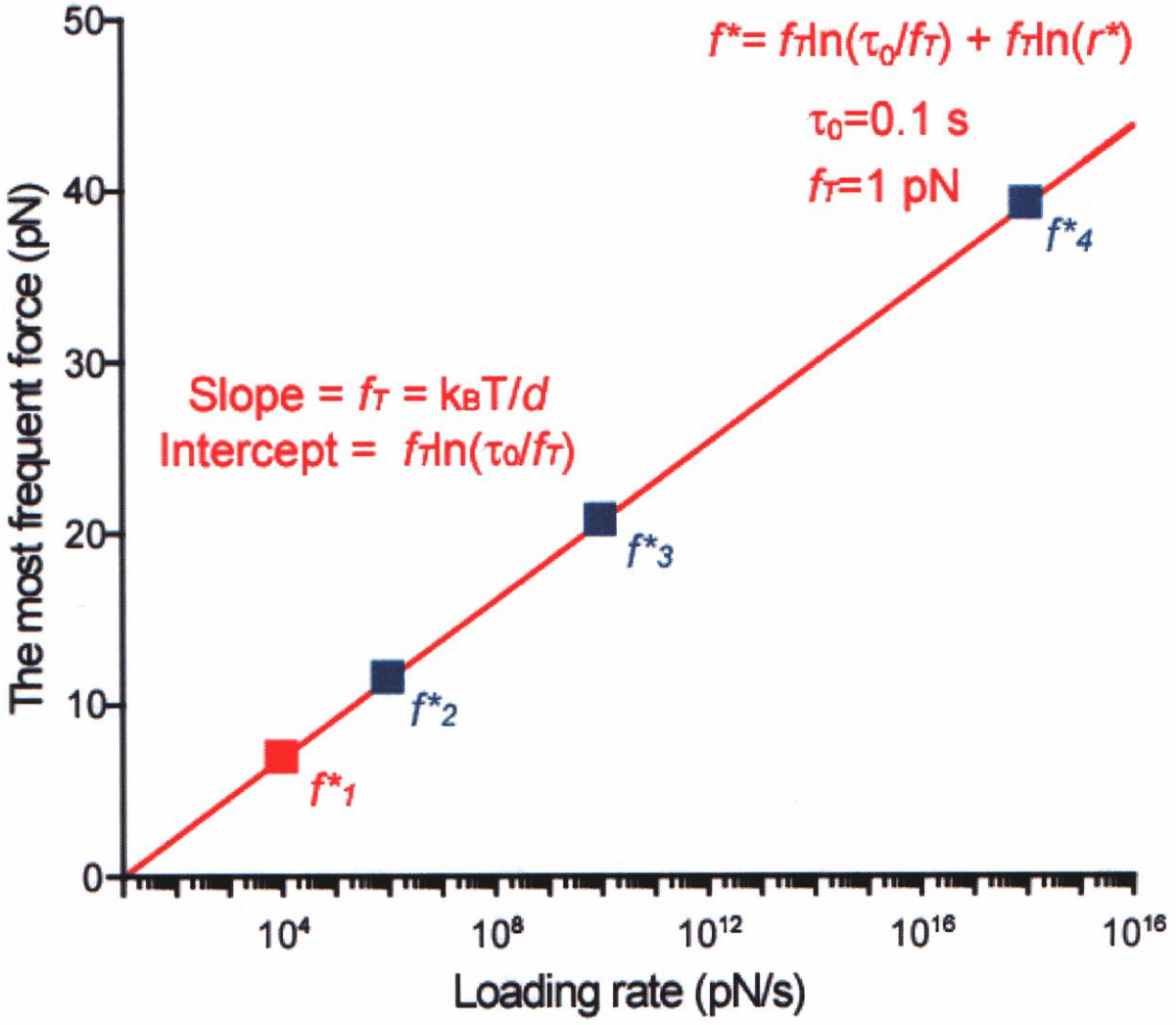

Figure 16 The most frequent force-loading rate plotting

The most frequent force on bond strength distribution shown in **Figure 13b** were plotted against loading rate on a logarithmic scale. f^*, f^*_1, f^*_2, f^*_3 and f^*_4 with τ_0 = 0.1 s, and f_T = 1pN, linearly increase against loading rate on a logarithmic scale. The most frequent force on bond strength distribution is written by solving $\partial p(f)/\partial f = 0$ as $f^* = f_T \ln(\tau_0 / f_T) + f_T \ln(r^*)$. Thus, on the most frequent force-loading rate plotting the slope, f_T is related only to d ($f_T = k_B T / d$), while the intercept, f^*_0, is related to d and τ_0 ($f^*_0 = f_T \ln(\tau_0 / f_T)$, where $f_T = k_B T / d$).

3.2. Bound state parameters

3.2.1. Lifetime

What does the lifetime obtained from single molecule bond strength measurement and analysis represent? To demonstrate the behaviour of ideal simple bonds, the forces needed to extract single diC14 lipids from the surface of a lipid (cholesterol vesicle) were measured(Evans and Ludwig 2000; Ludwig and Evans 2000). The lifetime obtained from the bond strength measurement and analysis at a high force region for diC14 lipid anchoring was ≈ 30 seconds. This lifetime is fifty-fold shorter than the lifetime for similar PEG-biotinylated diC14 lipids from lipid vesicles in solution(Silvius and Zuckermann 1993). To demonstrate complex molecular bond behaviour as proteins, the forces needed to break the interaction between single molecules of biotin-avidin were also measured. The maximum lifetime obtained from the bond strength measurement and analysis at the high force region was ≈ 60s, which is also shorter compared than the lifetime of ≈ 200000 s obtained from ensemble measurements in solution(Merkel, Nassoy et al. 1999). The longer lifetime in solution was interpreted to mean that the molecular attraction near the binding site significantly prolongs association in solution yet and are still

to small to be detected in force measurements because forces overwhelm the peripheral interaction. However, recent lifetime measurements using constant and low applied external force or single molecule imaging showed that the lifetime obtained from bond strength measurement and analysis at the low force region corresponds directly to the observed lifetime in the absence of applied external force(Baumgartner, Hinterdorfer et al. 2000; Baumgartner, Schutz et al. 2003; Bayas, Leung et al. 2006)(Tsukasaki et al., unpublished data). Although further studies are needed to clarify the differences between single molecule and multiple molecules measurements, it appears that the lifetime obtained from bond strength measurement and analysis in the low force region approximately reflects the lifetime between single molecules in solution.

3.2.2. Bond length

Similar to the question regarding lifetime, what does the bond length reflect? An ideal bond model can be seen in the case of diC14 lipid anchoring. The single molecule bond strength measurement and analysis showed that bond length was ≈ 1.95 nm, which was very near the half-thickness of a lipid-cholesterol membrane (2nm). This bond length was interpreted as the length of hydrophobic interaction between the diC14 lipid and lipid-cholesterol membrane, therefore, the bond length should be consistent with the length of diC14 lipid inserted in the membrane(Evans and Ludwig 2000; Ludwig and Evans 2000). Furthermore, as an example of simple multiple bonds the single molecule bond strength measurement and analysis of short DNA duplexes also has showed that the bond length correlated proportionately with the number of base pairs. Thus, the increase of bond length with number of base pairs were nicely demonstrated, resulting in ≈ N*0.116 nm(Strunz, Oroszlan et al. 1999). Namely, it is reasonable to take the bond length as the length achieved by the bond until the bond breaks. On the other hand, the bond length between protein molecules is much more complex. The bond length of biotin–streptavidin system was studied by bond

strength measurement and analysis. The result showed that there were two specific bond lengths corresponding to the points where different energy barriers exist. The first barrier was located at bond length of ≈ 0.12 nm and a second barrier, ≈ 0.5 nm. These two transition points are consistent with the locations of prominent chemical barriers, which was revealed by the molecular dynamics(Grubmuller, Heymann et al. 1996; Merkel, Nassoy et al. 1999). In the simulations of molecular dynamics, an initial displacement of less than 0.2 nm caused the biotin `head' (ureido ring) detach from a nest of hydrogen bonds, water bridges and non-polar interactions deep in the binding pocket, which consistent with the measurement (the first barrier at ≈ 0.12 nm). Next, at a distance of 0.5nm, the forces reached maximal values followed by sudden displacements of biotin, which was attributed to a rupture in a transient network of water bridges and hydrogen bonds. This is consistent again with the measurement (the second barrier at ≈ 0.5 nm). Finally, as biotin left the pocket, a prominent jump occurred at 1 nm attributed to hydrogen bonds (Merkel, Nassoy et al. 1999). Thus, the bond length of biotin–streptavidin system can be interpreted as the collection of three stages; 1. biotin `head' in the streptavidin pocket, 2. intermediate state 3. biotin

'head' outside the streptavidin pocket. This is a general view of the bond length of biotin–streptavidin system. The bond length for protein-bond is the length of protein-protein interaction but it is usual that the bond length were collection of bond length originated by different causes attributed to some physical or chemical interactions (bonds). Furthermore, even if the location of each bond responsible for the binding are known, it is difficult to understand the bond length characterized precisely, because the partition of force and the degree of cooperativity among binding sites is still unclear. Further experimental and theoretical work is necessary.

4. Relationship among multiple bonds

4.1. Multiple bound states between paired cadherins and paired nectins

4.1.1. Multiple bound states between paired cadherins

We first analyzed the bond strength, defined as the force necessary to break an interaction, of homo-*trans* interactions between paired E-cadherin chimera proteins (Cefs)(**Figure 7 and see Chapter 2**). **Figure 17** shows a bond strength histogram between paired Cefs obtained at 10^3 pN/s under an interaction probability of 0.21, in which most detachments (

$$\frac{(0.21)\exp(-0.21)}{1-\exp(-0.21)} > 89\%$$

based on Poisson statistics) were expected to be due to single molecules(Zhu, Long et al. 2002). We clearly resolved four bound states between paired Cefs as four distinct bond strength distributions, defining the 1st, 2nd, 3rd and 4th distributions as Cef_{1st}, Cef_{2nd}, Cef_{3rd} and Cef_{4th}, respectively. It is suggested that four independent bound states exist in the interaction between single molecules of paired Cefs. Fitting of bond strength distributions to the multiple bond strength probability density function

$$P(f)=\sum a_n p_n(f)$$

(Dotted black curve in **Figure 17**), where a_n are freely adjustable parameters to compensate the fractions of subpopulations, the bond strength probability density function

$$p_n(f) = \left(\frac{1}{r^* \tau_0}\right) \exp\left(\frac{f}{f_T}\right) \exp\left(-\frac{f_T}{r^* \tau_0}\right) \left(\exp\left(\frac{f}{f_T}\right) - 1\right)$$

(Blue, green, red and violet solid curves in **Figure 17** and **see Chapter 3**) and n is the number of subpopulations, resulted in two bound state parameters, lifetimes, τ_0, and bond lengths, d, for the four bound states; where f is the bond strength,

$$f_T = \frac{k_B T}{d}$$

, where k_B is Boltzman's constant, T is the absolute temperature, d is the bond length, r^* is the loading rate, τ_0 is the lifetime in the absence of applied external force. The most frequent force of the bond strength distribution, f^*, is related to τ_0 and d (

$$f^* = f_T \ln\left(\frac{\tau_0}{f_T}\right) + f_T \ln(r^*)$$

,

$$f_T = \frac{k_B T}{d}$$

)(**Figure 14**, **Figure 16** and **see Chapter 3**) while the standard deviation of the bond strength distribution, σ, is related only to d (

$$\sigma \approx 2.12\left(\frac{k_B T}{d}\right)$$

)(**Figure 15** and **see Chapter 3**). The bound state parameters were τ_0 = 0.107 ± 0.008 s and d = 0.71 ± 0.02 nm for Cef_{1st}, τ_0 = 1.68 ± 0.29 s and d = 0.62 ± 0.02 nm for Cef_{2nd}, τ_0 = 136 ± 69 s and d = 0.79 ± 0.04 nm for Cef_{3rd} and τ_0 = 273000 ± 191000 s and d = 1.1 ± 0.04 nm for Cef_{4th}; approximating those previously obtained from the relationship between loading rate and the most frequent force measured by BFP system(Perret, Leung et al. 2004). These data demonstrate that the bond strength distribution measured by our IFM system reflects the unbinding nature for each bound state, which follows a Markov process(Evans 2001). The appearance of multiple bond strength distributions between paired cadherins may be attributed to multiple types of bonds due to the heterogeneity of the coated molecules or mixed populations of single, double, triple etc molecular complexes. However, the appearance of multiple bond strength distributions was preserved in all experimental preparations, even when the protein concentration was changed. Thus, we concluded that the appearance of multiple bond strength distributions in bond strength histograms corresponds to multiple bound states for the interaction between single molecules of paired Cefs.

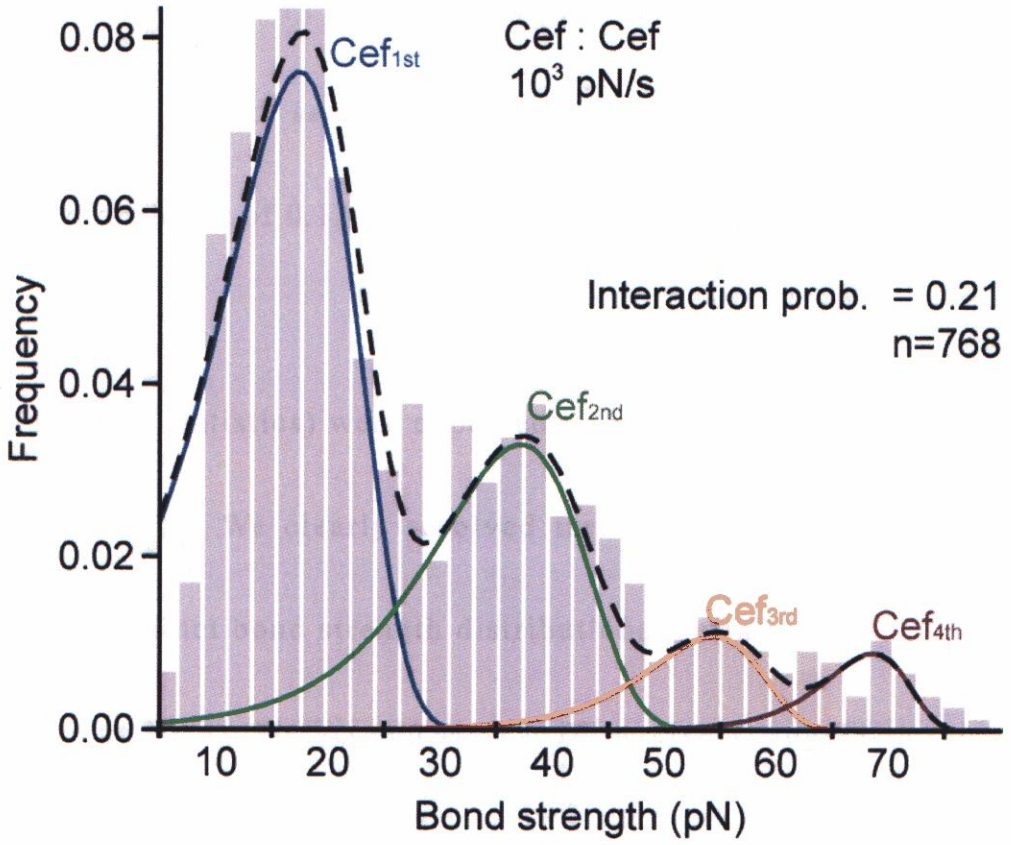

Figure 17 Bond strength histogram between paired Cefs

A bond strength histogram between paired Cefs obtained at 10^3 pN/s under an interaction probability of 0.21 (n = 768). Blue, green, red and violet solid curves represent the fittings including parameters to compensate for the fractions of subpopulations of the bond strength probability density function, $p(f) = (1/(r * \tau_0))\exp(f / f_T)\exp(-(f_T /(r * \tau_0))(\exp(f / f_T) - 1))$ (**See Figure 13b** and **Chapter 3**). Dotted Black curve represents the sum of four bond strength probability densities, defining the 1st, 2nd, 3rd and 4th distributions as Cef_{1st}, Cef_{2nd}, Cef_{3rd} and Cef_{4th}, respectively.

4.1.2. Multiple bound states between paired nectins

Figure 18 shows a bond strength histogram of hetero-*trans* interactions between nectin-1 chimera protein (Nef-1) and nectin-3 chimera protein (Nef-3) (**Figure 7** and **see Chapter 2**) obtained at 10^3 pN/s under an interaction probability of 0.12, in which most detachments (

$$\frac{(0.12)\exp(-0.12)}{1-\exp(-0.12)} > 94\%$$

based on Poisson statistics) were expected to be due to single molecules(Zhu, Long et al. 2002). We clearly resolved three bound states between paired Nefs as three distinct bond strength distributions, defining the 1st, 2nd and 3rd distributions as Nef_{1st}, Nef_{2nd} and Nef_{3rd}, respectively, suggesting that three independent bound states exist in the interaction between single molecules of paired Nefs. Fitting of bond strength distribution to the multiple bond strength probability density function (Dotted black curve, blue, green and red solid curves in **Figure 18 and see Chapter 3**) again resulted in the two bound state parameters, τ_0 and d, for the three bound states. The appearance of multiple bond strength distributions between paired nectins may be attributed to multiple types of bonds due to the heterogeneity of the coated molecules or mixed populations of single, double, triple etc molecular complexes.

However, the appearance of multiple bond strength distributions was preserved in all experimental preparations, even when the protein concentration was changed. Thus, we concluded that the appearance of multiple bond strength distributions in bond strength histograms corresponds to multiple bound states for the interaction between single molecules of paired Nefs.

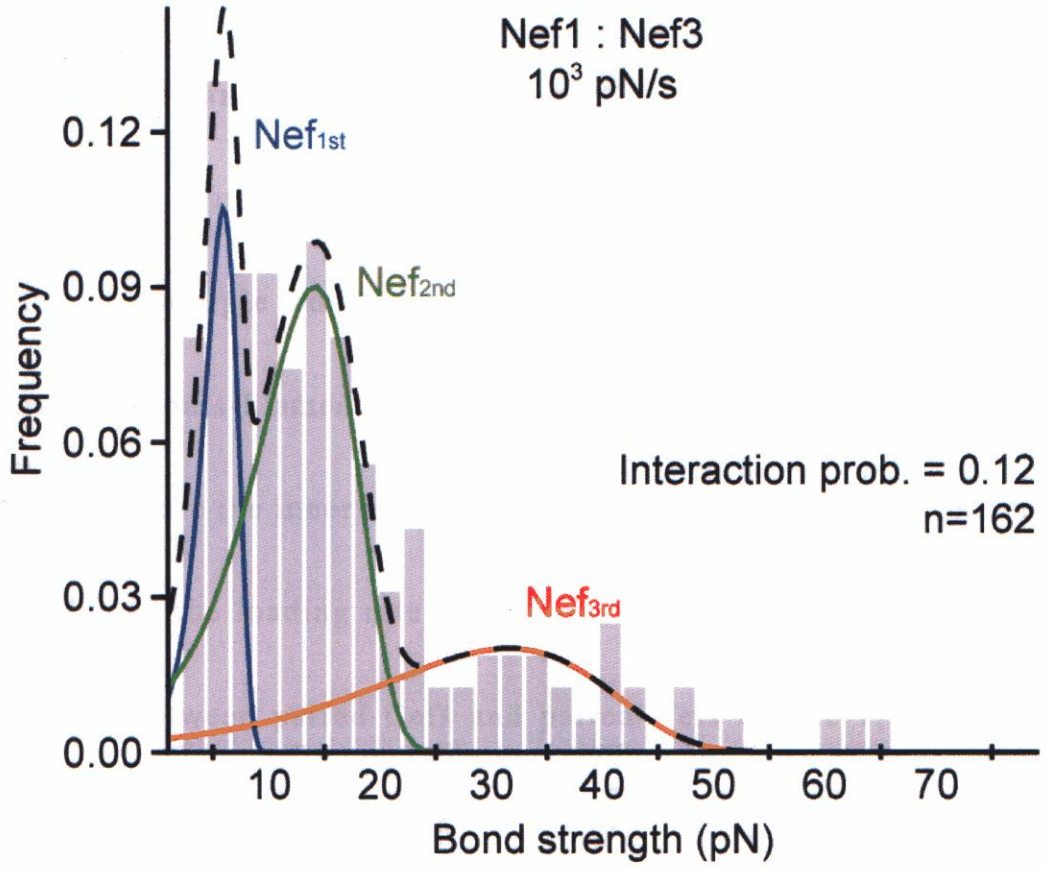

Figure 18 Bond strength histogram between paired Nefs

A bond strength histogram between paired Nefs obtained at 10^3 pN/s under an interaction probability of 0.12 (n = 162). Blue, green and red solid curves represent the fittings including parameters to compensate for the fractions of subpopulations of the bond strength probability density function, $p(f) = (1/(r*\tau_0))\exp(f/f_T)\exp(-(f_T/(r*\tau_0))(\exp(f/f_T)-1))$ (**See Figure 13b** and **Chapter 3**). Dotted black curve represents the sum of three bond strength probability densities, defining the 1st, 2nd and 3rd distributions as Nef_{1st}, Nef_{2nd} and Nef_{3rd}, respectively.

4.2. Multiple bonds act as cooperative bonds in cadherin and uncooperative bonds in nectin

4.2.1. Loading rate dependency of bound state parameters between paired cadherins and paired nectins

Multiple bound states between paired cadherins and paired nectins can be attributed to multiple bonds existing on multiple tandem aligned domain structures(Chappuis-Flament, Wong et al. 2001; Yasumi, Shimizu et al. 2003). In order to explore the inner world of bound states involving multiple domains, we investigated the loading rate dependency of bound state parameters at all bound states between paired Cefs and paired Nefs (**Table 1**, **Figure 19** and **Figure 20**).

4.2.1.1. Loading rate dependency of bound state parameters between paired cadherins

Lifetimes between paired Cefs were approximately constant against an increasing loading rate at all bound states (Blue, green, red and violet plots and solid curves in **Figure 19a**). Bond lengths between paired Cefs were also approximately constant against an increasing loading rate for all bound

states (Blue, green, red and violet plots and solid curves in **Figure 19b**).

Loading rate	10 pN/s			10^2 pN/s			10^3 pN/s			10^4 pN/s		
Bond state	τ_0 (s)	d (nm)	f^* (pN)	τ_0 (s)	d (nm)	f^* (pN)	τ_0 (s)	d (nm)	f^* (pN)	τ_0 (s)	d (nm)	f^* (pN)
Cef_{1st}				0.11 ± 0.003	0.64 ± 0.03	3.5 ± 0.05	0.11 ± 0.008	0.71 ± 0.02	16.9 ± 0.7	0.11 ± 0.03	0.59 ± 0.05	35.5 ± 4.2
Cef_{2nd}				1.69 ± 0.17	0.77 ± 0.03	18.5 ± 1.0	1.68 ± 0.29	0.62 ± 0.02	36.8 ± 2.1	4.23 ± 2.83	0.76 ± 0.07	49.0 ± 7.6
Cef_{3rd}				120 ± 48.8	0.88 ± 0.05	36.7 ± 3.6	136 ± 68	0.79 ± 0.04	53.0 ± 5.1	300 ± 139	0.88 ± 0.03	62.6 ± 4.0
Cef_{4th}				335000 ± 273000	1.19 ± 0.06	55.8 ± 5.5	273000 ± 191000	1.10 ± 0.04	68.2 ± 5.2	400000 ± 102000	1.2 ± 0.01	74.2 ± 1.8
Nef_{1st}	0.90 ± 0.11	7.97 ± 0.80	1.5 ± 0.2	0.30 ± 0.03	5.25 ± 0.17	2.9 ± 0.1	0.08 ± 0.04	2.71 ± 0.40	6.0 ± 1.4	0.01 ± 0.001	1.18 ± 0.06	12.2 ± 0.8
Nef_{2nd}	1.66 ± 0.39	4.32 ± 0.63	2.7 ± 0.5	0.45 ± 0.03	2.33 ± 0.053	5.8 ± 0.2	0.11 ± 0.01	0.87 ± 0.02	15.0 ± 0.6	0.02 ± 0.001	0.44 ± 0.01	27.2 ± 1.1
Nef_{3rd}	1.71 ± 0.28	1.73 ± 0.26	4.7 ± 0.8	1.10 ± 0.14	1.12 ± 0.05	12.5 ± 0.8	0.21 ± 0.04	0.41 ± 0.03	30.4 ± 3.1	0.03 ± 0.01	0.18 ± 0.02	60.7 ± 12.2

Table 1 Bound state parameters and the most frequent force

Bound state parameters and the most frequent force of all bound states, from Cef_{1st} to Cef_{4th} and from Nef_{1st} to Nef_{3rd}, at all loading rate, ranging from 10^2 pN/s to 10^4 pN/s for paired Cefs and from 10 pN/s to 10^4 pN/s for paired Nefs, are presented as mean ± s.e.m., τ_0, the lifetimes in the absence of applied force; d, the bond lengths; f^*, the most frequent force.

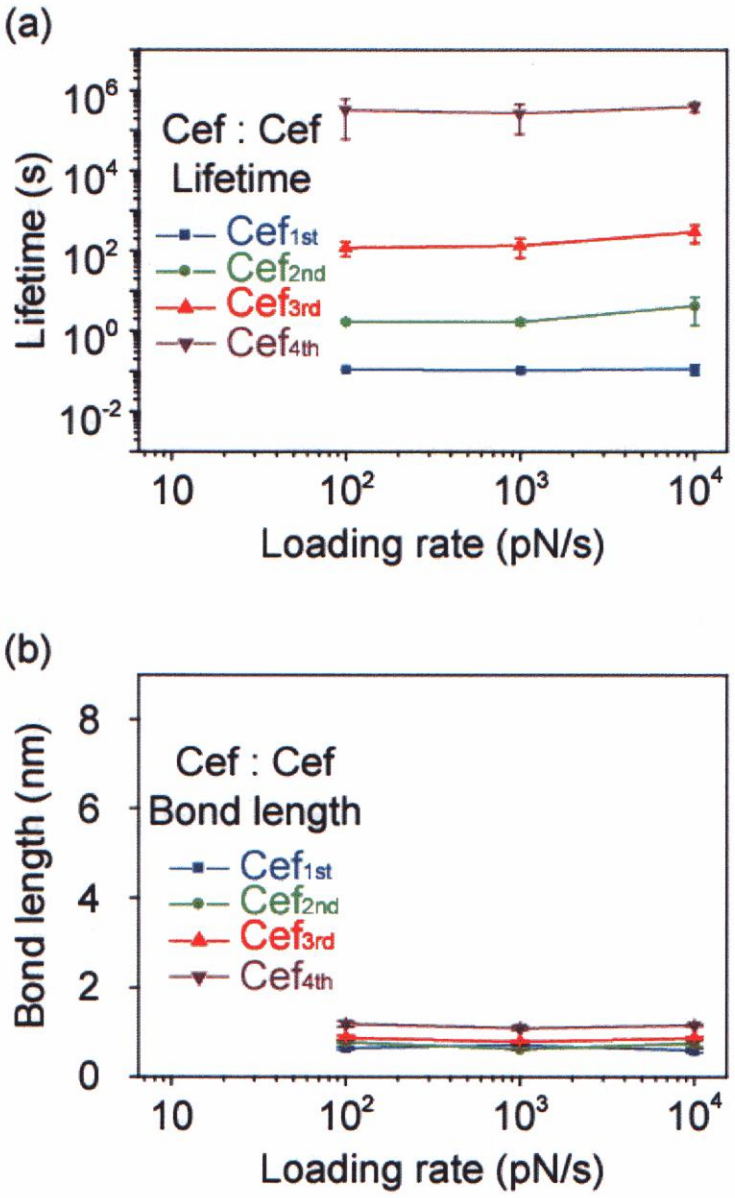

Figure 19 Loading rate dependency of bound state parameters between paired Cefs

(**a**) Loading rate dependency of lifetimes between paired Cefs. Lifetimes (mean ± s.e.m.) for all bound states between paired Cefs were plotted against loading rate on a logarithmic scale (Blue squares, Cef_{1st}; green circles, Cef_{2nd}; red triangles, Cef_{3rd}; violet inversed triangles, Cef_{4th}). (**b**) Loading rate dependency of bond lengths between paired Cefs. Bond lengths (mean ± s.e.m.) for all bound states between paired Cefs were plotted against loading rate on a logarithmic scale (Blue squares, Cef_{1st}; green circles, Cef_{2nd}; red triangles, Cef_{3rd}; violet inversed triangles, Cef_{4th}). Unseen symbols and lines of any colors are due to superimposition.

4.2.1.2. Loading rate dependency of bound state parameters between paired nectins

On the other hand, lifetimes between paired Nefs slightly decreased against an increasing loading rate for all bound states (Blue, green and red plots and solid curves in **Figure 20a**). Bond lengths between paired Nefs markedly decreased against an increasing loading rate for all bound states (Blue, green and red plots and solid curves in **Figure 20b**). This difference in loading rate dependency of bound state parameters between paired Cefs and paired Nefs suggests that behaviour of multiple bonds existing on the multiple tandem aligned domains differs between cadherins and nectins.

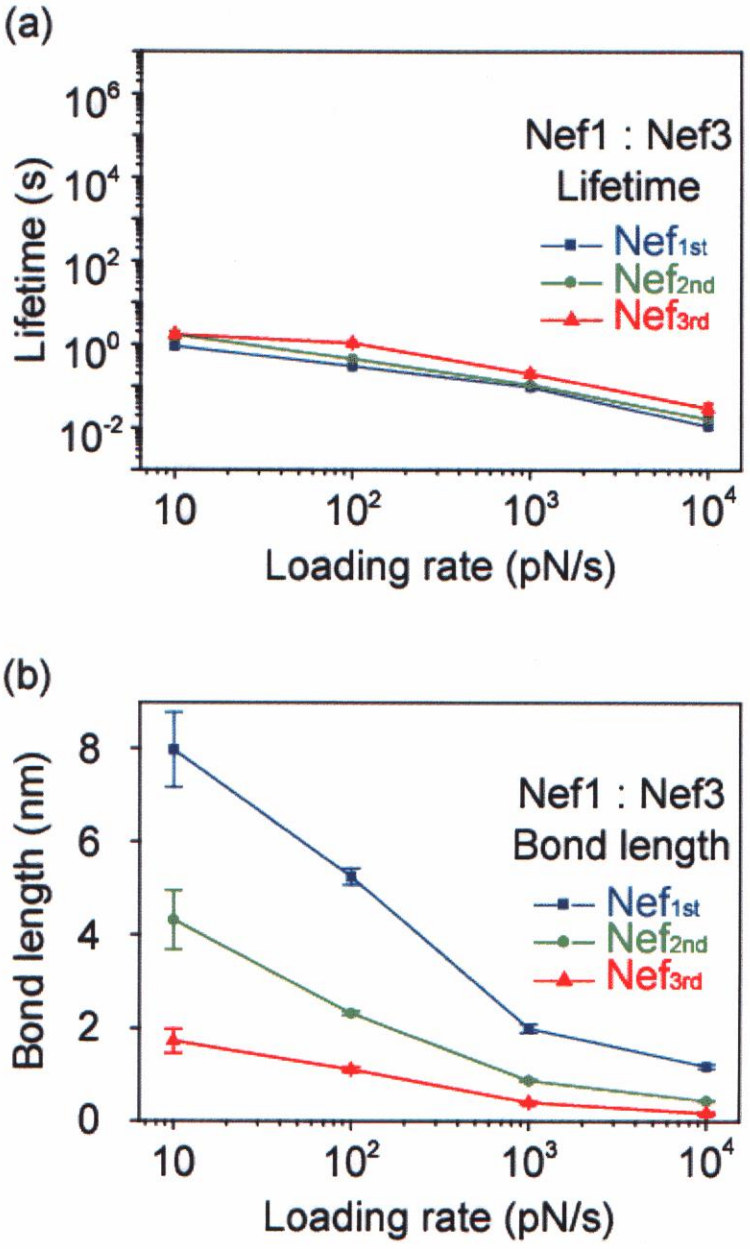

Figure 20 Loading rate dependency of bound state parameters between paired Nefs

(**a**) Loading rate dependency of lifetimes between paired Nefs. Lifetimes (mean ± s.e.m.) for all bound states between paired Nefs were plotted against loading rate on a logarithmic scale (Blue squares, Nef_{1st}; green circles, Nef_{2nd}; red triangles, Nef_{3rd}). (**b**) Loading rate dependencies of bond lengths between paired Nefs. Bond lengths (mean ± s.e.m.) for all bound states between paired Nefs were plotted against loading rate on a logarithmic scale (Blue squares, Nef_{1st}; green circles, Nef_{2nd}; red triangles, Nef_{3rd}). Unseen symbols and lines of any colors are due to superimposition.

4.2.2. Loading rate dependency of the most frequent force between paired cadherins and paired nectins

The relationships between loading rate and bound state parameters also emerged when comparing the most frequent force with loading rate on a logarithmic scale (**Table 1**, **Figure 21** and **Figure 22**). Here, the slope, f_T, is related only to d (

$$f_T = \frac{k_B T}{d}$$

), while the intercept, f^*_0, is related to τ_0 and d (

$$f^*_0 = f_T \ln\left(\frac{f_T}{\tau_0}\right),$$

$$f_T = \frac{k_B T}{d}$$

)(**Figure 14**, **Figure 16** and **see Chapter 3**).

4.2.2.1. Loading rate dependency of the most frequent force between paired cadherins

As expected from loading rate independency of bound state parameters between paired Cefs, the most frequent force linearly increased with an increasing loading rate on a logarithmic scale for all bound states (Blue, green, red and violet plots and solid linear curves in **Figure 21**). This result

suggests that multiple bonds existing on multiple tandem aligned domains of cadherins act as a macro-single bond, that is, they are cooperative bonds.

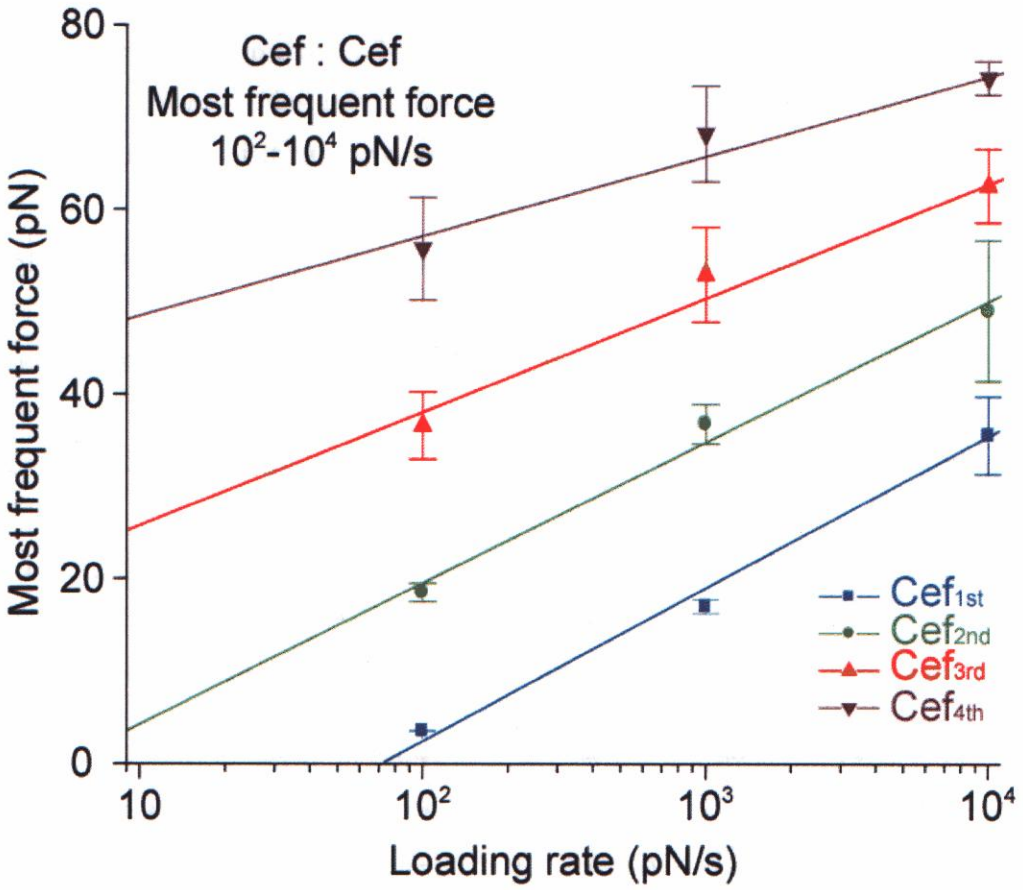

Figure 21 Loading rate dependency for the most frequent force between paired Cefs

The most frequent force (mean ± s.e.m.) for all bound states between paired Cefs were plotted against loading rate on a logarithmic scale (blue squares, Cef_{1st}; green circles, Cef_{2nd}; red triangles, Cef_{3rd}; violet inversed triangles, Cef_{4th}). Blue, green, red and violet linear solid curves represent the fittings of the relational expression between the most frequent force and loading rate, $f^* = f_T \ln(\tau_0 / f_T) + f_T \ln(r^*)$ (**see Figure 14**, **Figure 16** and **Chapter 3**).

4.2.2.2. Loading rate dependency of the most frequent force between paired nectins

In contrast, as expected from the loading rate dependency of bound state parameters between paired Nefs, the most frequent force nonlinearly increased against an increasing loading rate on a logarithmic scale for all bound states (Blue, green and red plots in **Figure 22**). This nonlinear relationship matched well with the theoretical curve shows multiple uncooperative bonds sequentially unbind (Blue, green and red solid curves in **Figure 22 and see Chapter 3**)(Evans 2001; Evans, Leung et al. 2001), as determined from the relationship among bound state parameters and the most frequent forces at all loading rates,

$$f^* = f_T \ln\left(\frac{\tau_0}{f_T}\right) + f_T \ln(r^*),$$

$$f_T = \frac{k_B T}{d}$$

(Dotted blue, green and red linear curves in **Figure 22 and see Chapter 3**). This nonlinear relationship is similar to those of macromolecular zippers previously observed(Merkel, Nassoy et al. 1999; Evans, Leung et al. 2001), suggesting that multiple bonds existing on multiple tandem aligned domains of nectins are uncooperative bonds that unbind sequentially like a zipper, that

is, they are a zipper-like multiply bonded system.

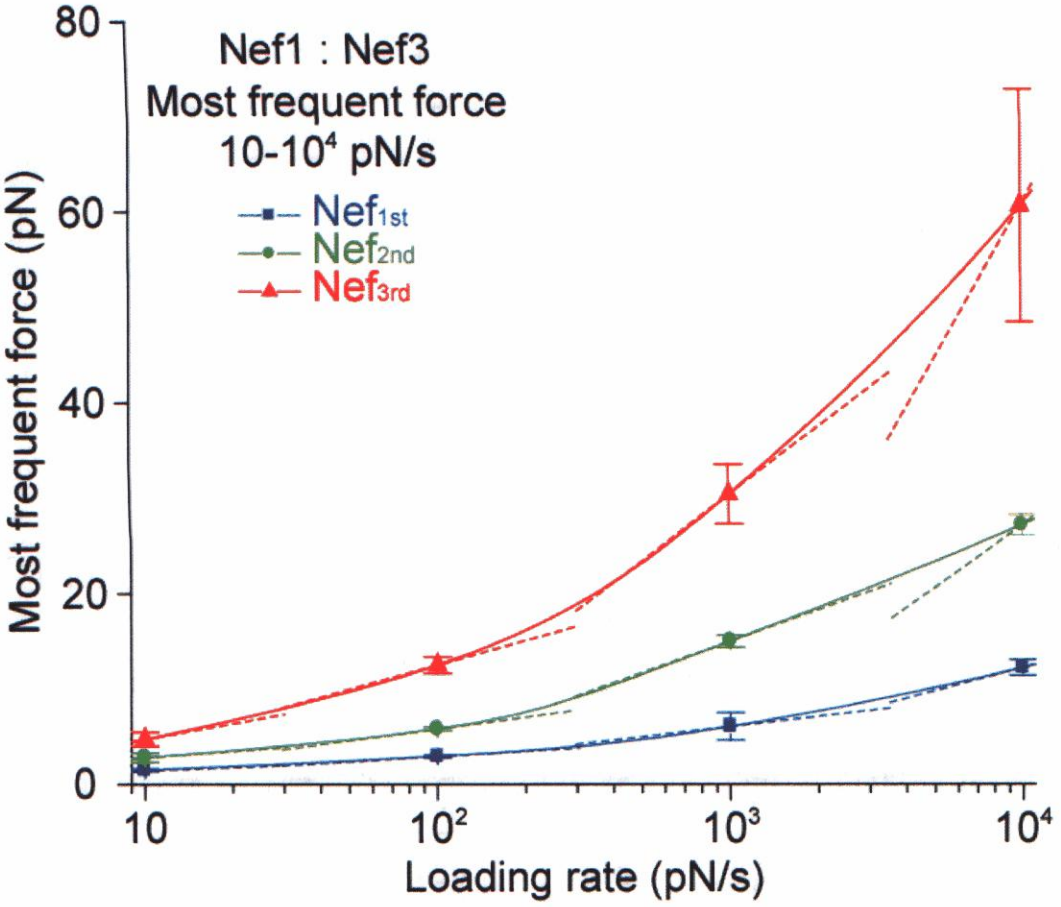

Figure 22 Loading rate dependency for the most frequent force between paired Nefs

The most frequent force (mean ± s.e.m.) for all bound states between paired Nefs were plotted against loading rate on a logarithmic scale (blue squares, Nef_{1st}; green circles, Nef_{2nd}; red triangles, Nef_{3rd}). Blue, green and red nonlinear solid curves represent the theoretical curves that multiple uncooperative bonds sequentially unbind (**see Chapter 3**). Dotted blue, green and red linear curves represents the relationship between lifetime and bond length and most frequent force obtained from each bond strength distribution, $f^* = f_T \ln(\tau_0 / f_T) + f_T \ln(r^*)$, $f_T = k_B T / d$ (**See Figure 14**, **Figure 16** and **Chapter 3**).

5. Multiple bonds configuration

In order to confirm how multiple tandem aligned domain structures involve multiple bound states between paired cadherins and paired nectins, we investigated the relationship between bound state parameters and multiple bound states for paired Cefs and paired Nefs (**Table 1**, **Figure 23 and Figure 26**).

5.1 Relationship of lifetimes among multiple bound states between paired cadherins and paired nectins

Lifetimes between paired Cefs increased in an exponential fashion from bound state Cef_{1st} to Cef_{4th} at all loading rates (Blue, green and red plots and solid curves in **Figure 23a**). When multiple bonds act as cooperative bonds, the lifetime of the composite bond is scaled by the sum of the individual bond barrier energy. Total lifetime of the composite bond increases approximately in an exponential fashion as cooperative bonds are added according to an approximation,

$$\tau_0(n) \approx (\sum \tau_{Dn}) \exp((\sum E_n)/k_B T)$$

, where $\tau_0(n)$ is the total lifetime of a composite bond with n cooperative

bonds in the absence of applied external force, n is the number of cooperative bonds, τ_{Dn} is the diffusive relaxation time for the individual bond, E_n is the barrier energy height for individual bond($\sum \tau_{Dn}$ is based on a putative model where the diffusive relaxation time is also scaled with the sum of the individual bond) (**Figure 24**)(Strunz, Oroszlan et al. 1999; Evans 2001). Thus, this result supports the cooperative behaviour between multiple bonds existing on tandem aligned domains of cadherins as shown in **Figure 19** and **Figure 21**, and furthermore suggests that the number of tandem aligned domains interacting increases in order from bound state Cef_{1st} to Cef_{4th}. On the other hand, lifetimes on a logarithmic scale between paired Nefs were approximately constant from bound state Nef_{1st} to Nef_{3rd} at all loading rates (Blue, green, red and violet plots and solid curves in **Figure 23b**). When multiple bonds act as uncooperative bonds in a zipper-like multiply bonded system, the total lifetime of the composite bond is scaled by the sum of individual bond lifetimes. Total lifetime of the composite bond does not change in an exponential fashion even when uncooperative bonds are added according to an approximation,

$$\tau_0(n) \approx \sum \tau_{0n}$$

, where $\tau_0(n)$ is the total lifetime of a composite bond with n uncooperative bonds in the absence of applied external force, n is the number of uncooperative bonds, τ_{0n} is the lifetime for individual bonds in the absence of applied external force (**Figure 25**)(Merkel, Nassoy et al. 1999; Evans 2001; Evans, Leung et al. 2001). Thus, this result supports uncooperative behaviour of multiple bonds existing on tandem aligned domains of nectins as shown in **Figure 20** and **Figure 22**.

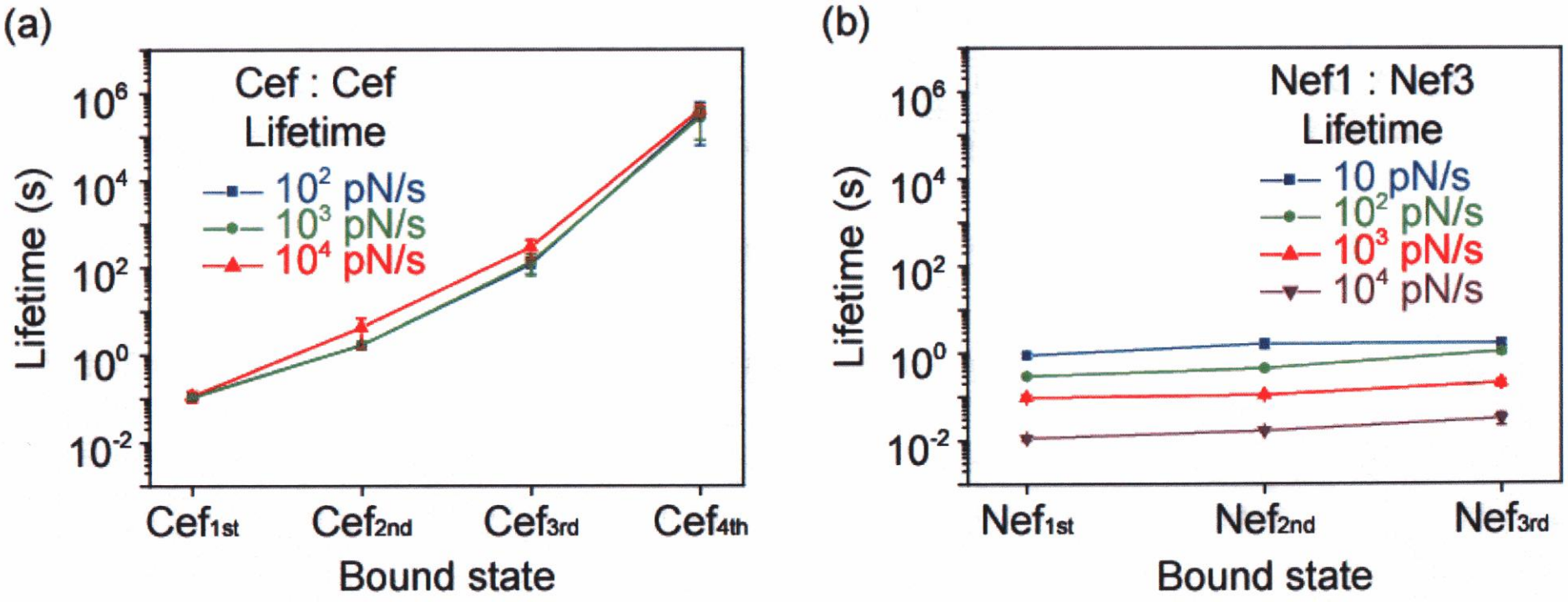

Figure 23 Relationship of lifetimes among multiple bound states

Relationship of lifetimes among multiple bound states between paired Cefs (a) and paired Nefs (b). Lifetimes (mean ± s.e.m.) on a logarithmic scale between paired Cefs and paired Nefs were plotted in the order from bound state Cef_{1st} to Cef_{4th}. (a) and in the order from bound state Nef_{1st} to Nef_{3rd} (b) (a: blue squares, 10^2 pN/s; green circles, 10^3 pN/s; red triangles, 10^4 pN/s. b: blue squares, 10 pN/s; green circles, 10^2 pN/s; red triangles, 10^3 pN/s; violet inversed triangles, 10^4 pN/s). Unseen symbols and lines of any colors are due to superimposition.

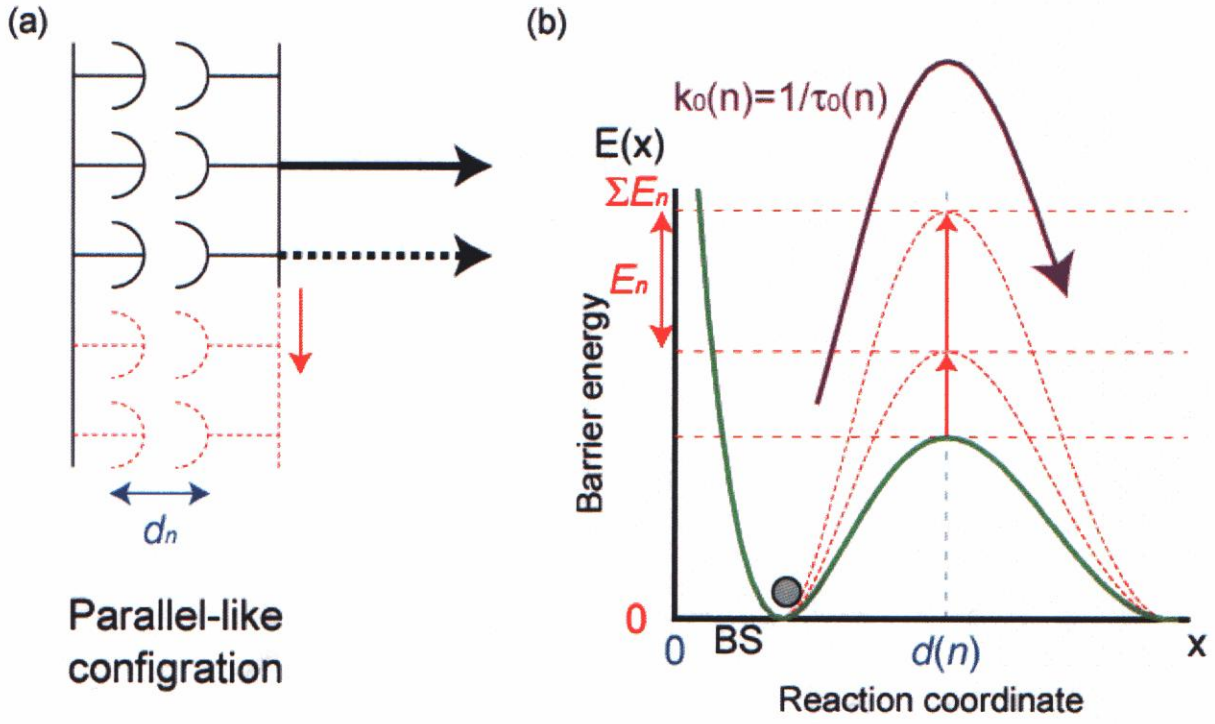

Figure 24 Theory for a cooperative parallel-like multiply bonded system

(a) Schematics of a parallel-like multiply bonded system. Black arrow and dotted black arrow represents the direction and location of applied force. (b) Conceptual energy landscape for a cooperative parallel-like multiply bonded system. When multiple bonds act as cooperative bonds, total lifetime of the composite bond is scaled by the sum of the individual bond barrier energy, i.e. $\tau_0(n) \approx (\Sigma\tau_{Dn})\exp((\Sigma E_n)/k_BT)$, where $\tau_0(n)$ is the total lifetime of the composite bond with n cooperative bonds in the absence of applied external force, n is the number of cooperative bonds, τ_{Dn} is the diffusive relaxation time for the individual bond, E_n is the barrier energy height for individual bond ($\Sigma\tau_{Dn}$ is based on a putative model where the diffusive relaxation time is also scaled with the sum of the individual bond). Thus, total lifetime of the composite bond increases approximately in an exponential fashion as cooperative bonds are added (red arrow in **a** and **b**). Total bond length of the composite bond is constant even when cooperative bonds are added (red arrow in **a** and **b**), i.e. $d(n) = d_n$, where $d(n)$ is the total bond length of the composite bond with n cooperative bonds, n is the number of cooperative bonds, d_n is bond length for the individual bond, assuming that bond length for the individual bond is constant, d_n=constant.

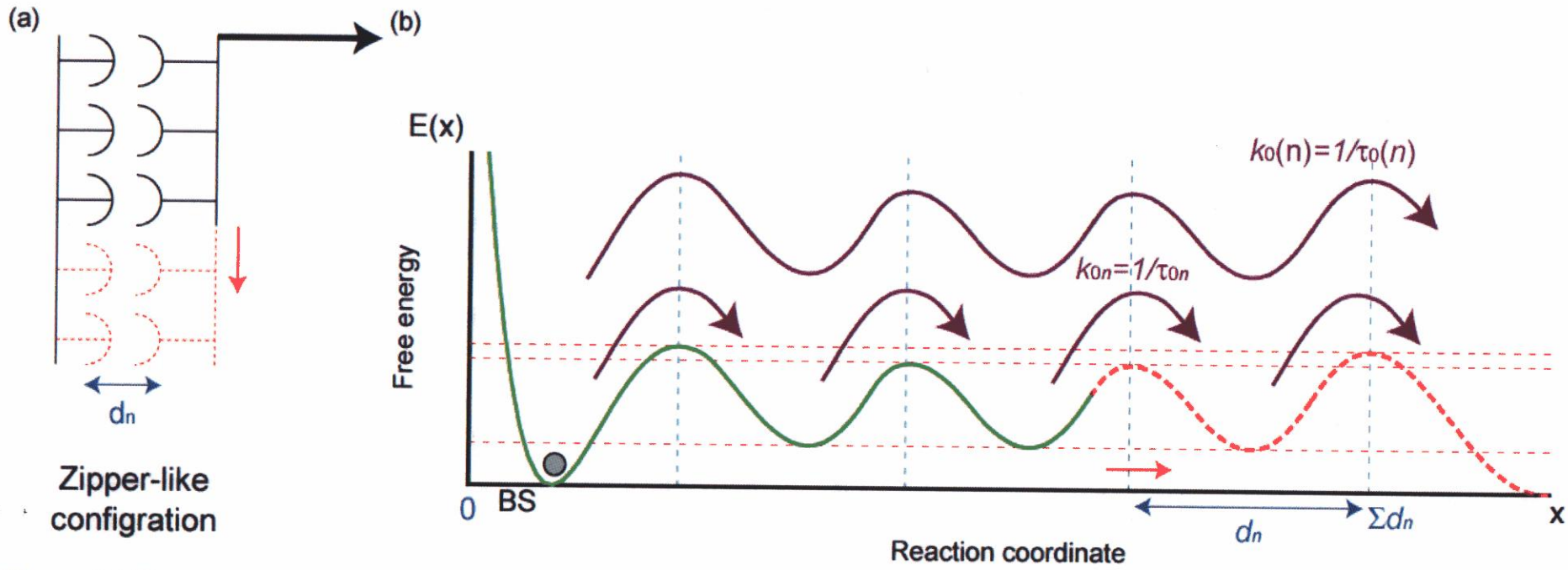

Figure 25 Theory for a uncooperative zipper-like multiply bonded system

(a) Schematics of a zipper-like multiply bonded system. Black arrow represents the direction and location of applied force. (b) Conceptual energy landscape for a uncooperative zipper-like multiply bonded system. When multiple bonds act as uncooperative bonds, total lifetime of the composite bond is scaled by the sum of individual bond lifetimes, i.e. $\tau_0(n) \approx \Sigma\tau_{0n}$, where $\tau_0(n)$ is the total lifetime of the composite bond with n uncooperative bonds in the absence of applied external force, n is the number of uncooperative bonds and τ_{0n} is the lifetime for the individual bond. Total lifetime of the composite bond does not increase approximately in an exponential fashion even when uncooperative bonds are added (red arrow in **a** and **b**). Total bond length of the composite bond is scaled by the sum of individual bond lengths, i.e. $d(n) \approx \Sigma d_n$, where $d(n)$ is the total bond length of the composite bond with n uncooperative bonds, n is the number of uncooperative bonds, d_n is bond length for the individual bond. Bond length is added as uncooperative bonds are added (red arrow in **a** and **b**).

5.2. Relationship of bond lengths among multiple bound states between paired cadherins and paired nectins

Bond lengths between paired Cefs did not significantly change from bound state Cef_{1st} to Cef_{4th} for all loading rates (Blue, green and red plots and solid curves in **Figure 26a**). In the case of cooperative, and a parallel-like multiply bonded system, bond length is constant even when cooperative bonds are added (**Figure 24**)(Evans 2001). Thus, this result suggests that multiple bonds existing on tandem aligned domains of cadherins use a parallel-like multiply bonded system. On the other hand, bond lengths between paired Nefs markedly increased from Nef_{3rd} to Nef_{1st} at all loading rates (blue, green, red and violet plots and solid curves in **Figure 26b**). In the case of uncooperative, and a zipper-like multiply bonded system, bond length increases as uncooperative bonds are added (**Figure 25**)(Merkel, Nassoy et al. 1999; Evans 2001; Evans, Leung et al. 2001). Thus, this result suggests that the number of tandem aligned domains of nectins involving a zipper-like multiply bonded system increases in order from bound state Nef_{3rd} to Nef_{1st}.

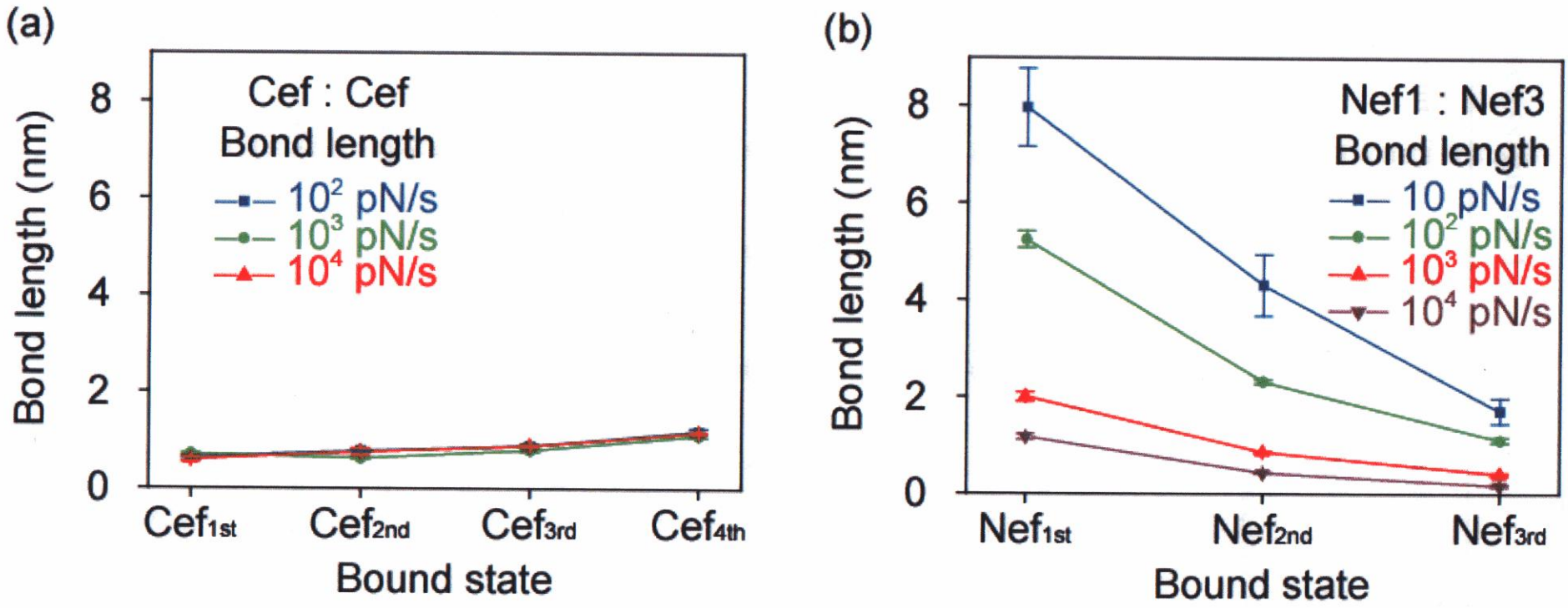

Figure 26 Relationship of bond lengths among multiple bound states

Relationship of bond lengths among multiple bound states between paired Cefs (a) and paired Nefs (b). Bond lengths (mean ± s.e.m.) between paired Cefs and paired Nefs were plotted in the order from bound state Cef_{1st} to Cef_{4th} (a) and in the order bound state from Nef_{1st} to Nef_{3rd} (b) (a: blue squares, 10^2 pN/s; green circles, 10^3 pN/s, red triangles; 10^4 pN/s. b: blue squares, 10 pN/s; green circles, 10^2 pN/s; red triangles, 10^3 pN/s; violet inversed triangles, 10^4 pN/s). Unseen symbols and lines of any colors are due to superimposition.

6. Discussion and conclusion

In this study, we clarified the difference in the dynamic mechanical interactions between paired nectins and paired cadherins at the single molecule level using high sensitive force measurement system with our IFM. The results indicate multiple tandem aligned domains of nectins act uncooperatively, as a zipper-like multiply bonded system while those of cadherins act cooperatively, as a parallel-like multiply bonded system. Based on these findings we constructed a model for multiple bound states between paired nectins and paired cadherins (**Figure 27 and Figure 28**).

6.1. Role of multiple bonds between paired nectins

We propose that multiple bound states between paired nectins correspond to antiparallel, hetero-*trans* interactions (**Figure 27a**). Thus, for Nef_{1st}, the first to third domains interdigitate; for Nef_{2nd}, the first and second domains interdigitate; and for Nef_{3rd}, the first domains interdigitate between paired nectins. The lifetimes did not significantly change with bound state from Nef_{1st} to Nef_{3rd} but the bond lengths did (**Figure 23b and 26b**). Therefore the stability of the bonds should not be very different between the first

domains, the first and second domains, and all three domains. This is consistent with mutational experiments(Miyahara, Nakanishi et al. 2000; Reymond, Fabre et al. 2001) and binding kinetics experiments(Yasumi, Shimizu et al. 2003) suggested that the involvement of the first domains is essential for *trans*-interaction between paired nectins. **Figure 27b** shows the unbinding manner of Nef_{1st} as an example of a bound state involving multiple tandem aligned domains of nectins. Multiple tandem aligned domains of nectins act as an uncooperative, zipper-like multiply bonded system resulting in all bonds unbinding sequentially in a zipper-like fashion.

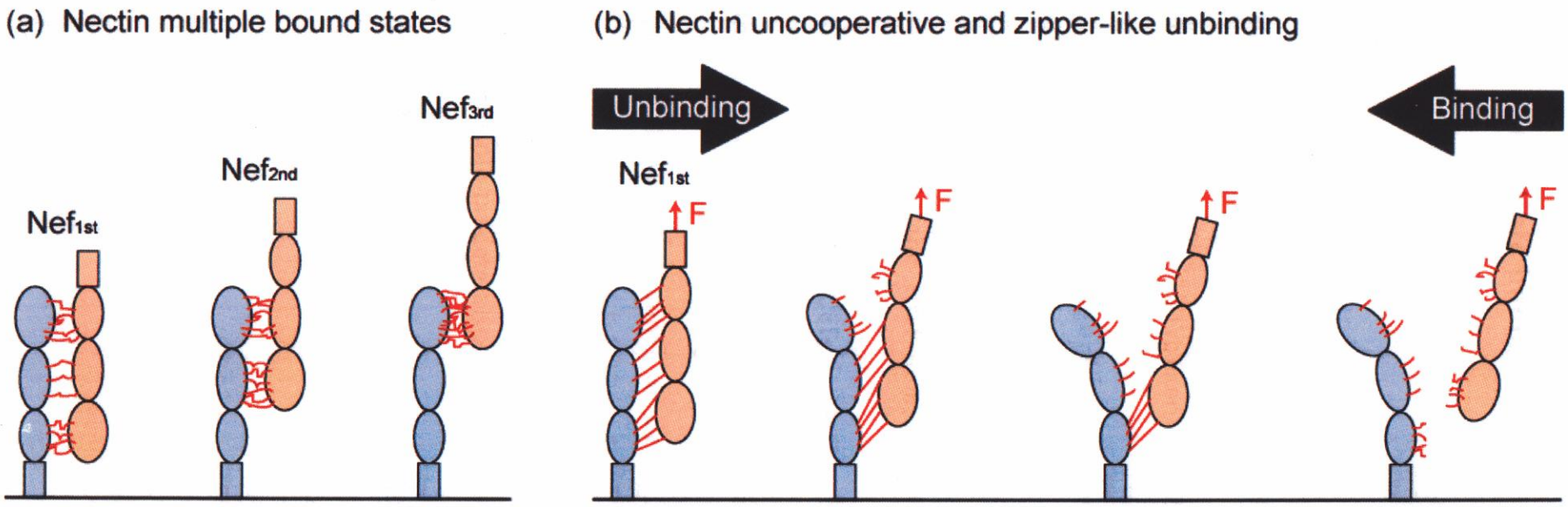

Figure 27 Behaviour of multiple bonds between paired nectins

(**a**) Multiple bound states between paired nectins. Red nonlinear lines represent multiple bonds on multiple tandem aligned domains. Multiple bound states, Nef_{1st}, Nef_{2nd} and Nef_{3rd}, are shown from left to right. (**b**) Uncooperative and zipper-like unbinding between paired nectins. The unbinding manner of bound state Nef_{1st} is shown as an example of a bound state involving multiple tandem aligned domains of nectins. Red linear lines represent multiple bonds on multiple tandem aligned domains stretched by an external force. Black arrows represent the direction of the unbinding and the binding reaction. Red arrows represent the direction of external force, F, applied in this study.

6.2. Role of multiple bonds between paired cadherins

In contrast, we propose a model that is a combination of the interdigitation hypothesis(Sivasankar, Brieher et al. 1999; Chappuis-Flament, Wong et al. 2001), where multiple domains of cadherins involve *trans*-interactions, and the strand dimer hypothesis(Troyanovsky 2005), where parallel cadherins interact with each other (**Figure 28a**). Here, the multiple bound states between paired cadherins correspond to parallel, homo-*trans* interactions. Thus, for Cef_{1st}, only the first domains overlap; for Cef_{2nd}, the first and second domains overlap; for Cef_{3rd}, the first to third domains overlap; and for Cef_{4th}, the first to forth domains overlap between paired cadherins. **Figure 28b** shows the unbinding manner of Cef_{4th} as an example of a bound state involving multiple tandem aligned domains of cadherins. Unlike nectins, cooperative multiple tandem aligned domains between paired cadherins act as a macro-single bond resulting in all bonds unbinding simultaneously.

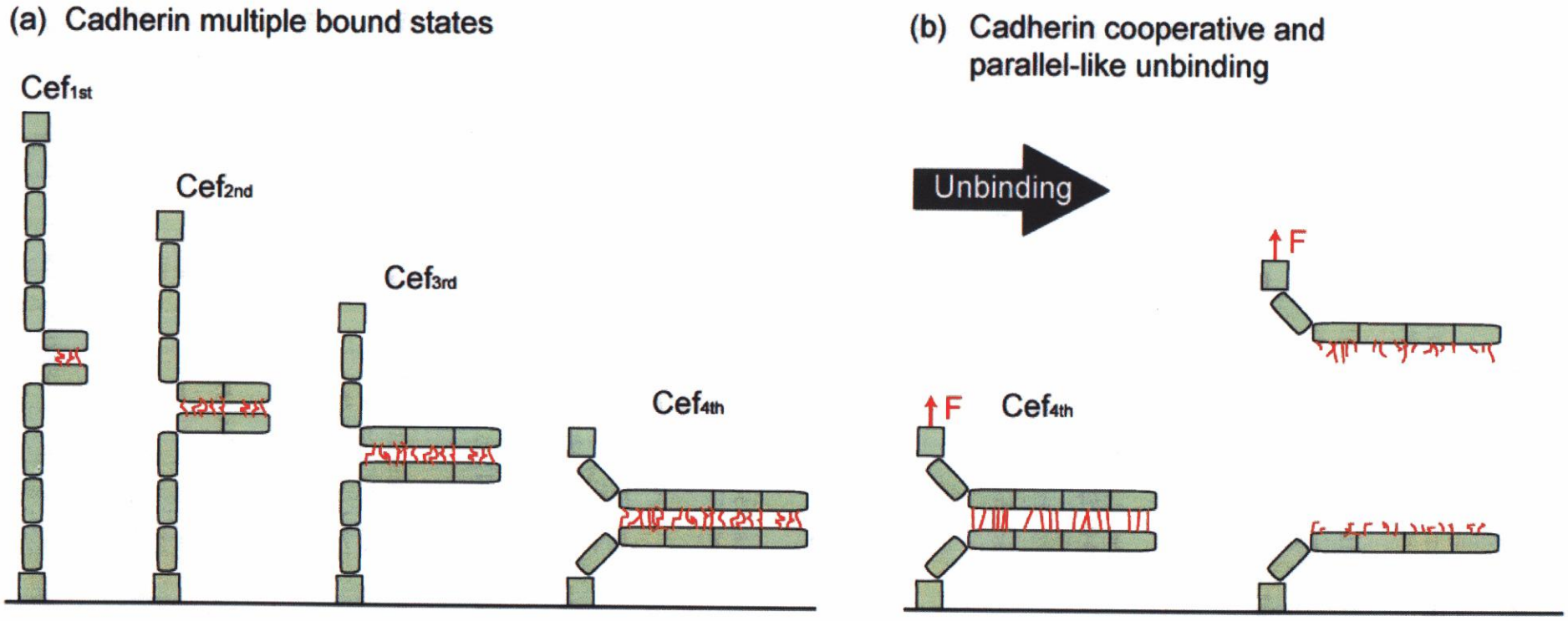

Figure 28 Behaviour of multiple bonds between paired cadherins

(**a**) Multiple bound states between paired cadherins. Red nonlinear lines represent multiple bonds on multiple tandem aligned domains. Multiple bound states, Cef_{1st}, Cef_{2nd}, Cef_{3rd} and Cef_{4th}, are shown from left to right. (**b**) Cooperative and parallel-like unbinding between paired cadherins. The unbinding manner of bound state Cef_{4th} is shown as an example of a bound state involving multiple tandem aligned domains of cadherins. Red linear lines represent multiple bonds on multiple tandem aligned domains stretched by an external force. Black arrows represent the direction of the unbinding reaction. Red arrows represent the direction of the external force, F, applied in this study.

6.3. A molecular based fork initiation and zipper model

How are the differences in dynamic characteristics between nectins and cadherins involved in the formation of cell-cell adhesions? Based on our results, we provide a molecular basis to the "fork initiation and zipper" hypothesis for the formation of cell-cell adhesions (**Figure 29**)(Takai and Nakanishi 2003; Irie, Shimizu et al. 2004). The uncooperative relation among multiple domains of nectins could be useful for fast bond formation. Multiple bonds between paired nectins are uncooperative and their lifetimes are relatively short, similar to that of the shortest bound states (Cef_{1st}) between paired cadherins(Perret, Leung et al. 2004) responsible for cell-cell adhesion specificity(Nose, Tsuji et al. 1990; Tamura, Shan et al. 1998). The random and fast binding and unbinding of nectins would be advantageous for the adaptive searching in the initial cell-cell exploratory recognition process. Cadherins showed much longer lifetimes than their nectin counterparts. For example, the lifetime of bound state Cef_{4th} was 10^5-10^7 folds as long as those of nectins due to the cooperative relation among multiple domains of cadherins. Thus, cadherins would play a key role in the formation of rigid and stable cell-cell adhesions. Since the cooperative relation among

multiple domains is expected to be mechanically rigid relation among multiple domains of cadherins as previously suggested(Pokutta, Herrenknecht et al. 1994; Sivasankar, Brieher et al. 1999; Baumgartner, Hinterdorfer et al. 2000), bond formation would be slow. In our model, nectins and E-cadherins are diffusely distributed on the free surface of the plasma membrane of migrating cells. When two migrating cells contact through their protrusions, nectins frequently bind and unbind each other at cell-cell contact sites. *Trans*-interactions of nectins induce the activation of cytoplasmic signaling (Cdc42), resulting in an increase in the number of filopodia and cell-cell contact sites like 'Fork initiation'. This is the cell-cell exploratory process by nectins (**Figure 29a**). Another cytoplasmic signaling (GTP-Rac) activated by either the *trans*-interactions of nectins or that of E-cadherin induces the formation of lamellipodia. The lamellipodia efficiently expand the cell-cell adhesion between the filopodia and via a slow reaction for the stable and rigid bond formation between *trans*-interactions of cadherins stabilize the cell-cell contact sites like 'Zipper'. This is the cell-cell zippering process by cadherins (**Figure 29b**). Ultimately, nectin-E-cadherin complex based Ajs are formed (**Figure 29c**).

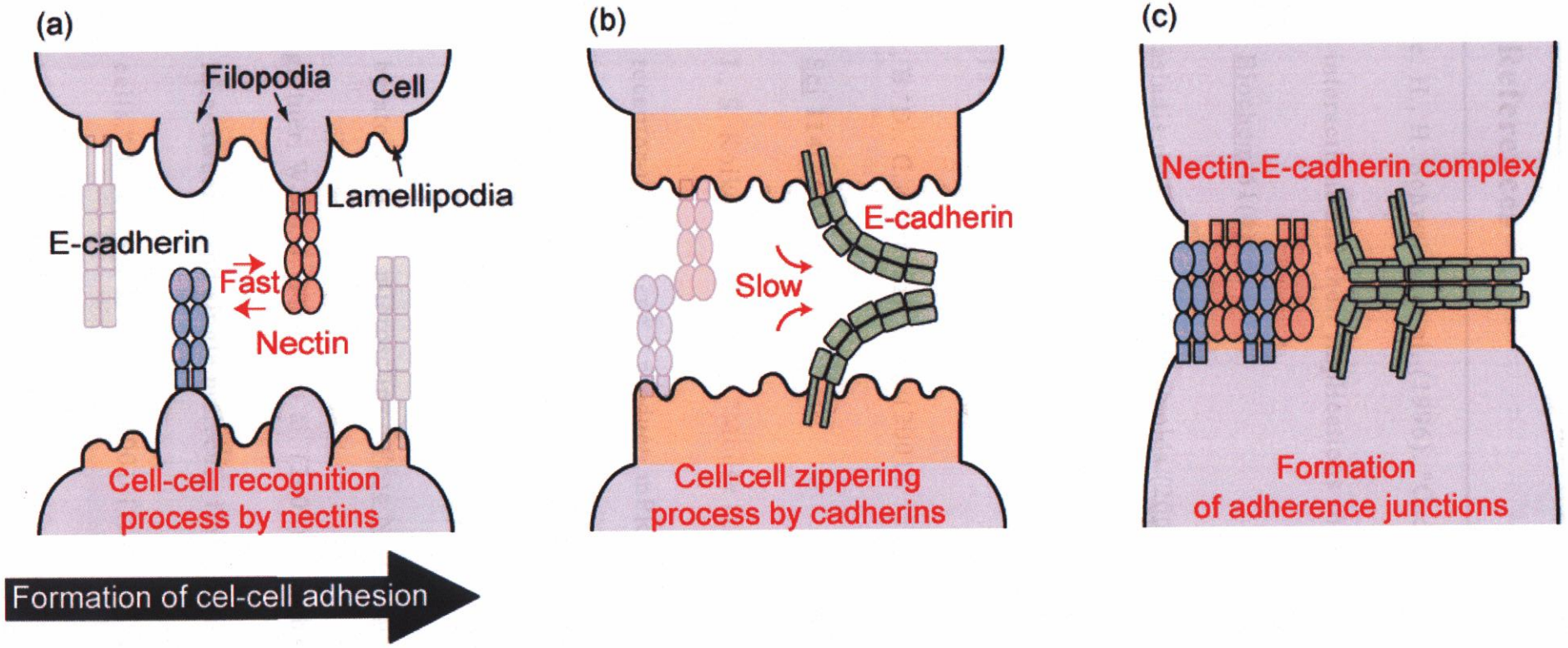

Figure 29 Bond strength measurement system

(**a**) Cell-cell exploratory recognition process by nectins. Gray regions, gray protrusions and orange protrusions represent cell, filopodia and lamellipodia, respectively. Red arrows represent the fast binding and unbinding reaction between paired nectins. E-cadherins are represented by weak colors. (**b**) Cell-cell zippering process by cadherins. Red arrows represent the slow reaction for the stable and rigid bond formation between paired cadherins. Nectins are represented by weak colors. (**c**) Formation of adherence junctions. Black arrow shows the direction of the formation of cell-cell adhesion.

7. References

Aberle, H., H. Schwartz, et al. (1996). "Cadherin-catenin complex: protein interactions and their implications for cadherin function." J Cell Biochem **61**(4): 514-23.

Anastasiadis, P. Z. and A. B. Reynolds (2000). "The p120 catenin family: complex roles in adhesion, signaling and cancer." J Cell Sci **113 (Pt 8)**: 1319-34.

Angst, B. D., C. Marcozzi, et al. (2001). "The cadherin superfamily." J Cell Sci **114**(Pt 4): 625-6.

Aoki, J., S. Koike, et al. (1997). "Mouse homolog of poliovirus receptor-related gene 2 product, mPRR2, mediates homophilic cell aggregation." Exp Cell Res **235**(2): 374-84.

Baumgartner, W., P. Hinterdorfer, et al. (2000). "Cadherin interaction probed by atomic force microscopy." Proc Natl Acad Sci U S A **97**(8): 4005-10.

Baumgartner, W., G. J. Schutz, et al. (2003). "Cadherin function probed by laser tweezer and single molecule fluorescence in vascular endothelial cells." J Cell Sci **116**(Pt 6): 1001-11.

Bayas, M. V., A. Leung, et al. (2006). "Lifetime measurements reveal kinetic

differences between homophilic cadherin bonds." Biophys J **90**(4): 1385-95.

Bell, G. I. (1978). "Models for the specific adhesion of cells to cells." Science **200**(4342): 618-27.

Binnig, G., C. F. Quate, et al. (1986). "Atomic force microscope." Physical Review Letters **56**(9): 930-933.

Boggon, T. J., J. Murray, et al. (2002). "C-cadherin ectodomain structure and implications for cell adhesion mechanisms." Science **296**(5571): 1308-13.

Brieher, W. M., A. S. Yap, et al. (1996). "Lateral dimerization is required for the homophilic binding activity of C-cadherin." J Cell Biol **135**(2): 487-96.

Chappuis-Flament, S., E. Wong, et al. (2001). "Multiple cadherin extracellular repeats mediate homophilic binding and adhesion." J Cell Biol **154**(1): 231-43.

Chu, Y. S., O. Eder, et al. (2006). "Prototypical type I E-cadherin and type II cadherin-7 mediate very distinct adhesiveness through their extracellular domains." J Biol Chem **281**(5): 2901-10.

Evans, E. (2001). "Probing the relation between force--lifetime--and chemistry in single molecular bonds." Annu Rev Biophys Biomol Struct **30**: 105-28.

Evans, E., A. Leung, et al. (2001). "Chemically distinct transition states govern rapid dissociation of single L-selectin bonds under force." Proc Natl Acad Sci U S A **98**(7): 3784-9.

Evans, E. and F. Ludwig (2000). "Dynamic strengths of molecular anchoring and material cohesion in fluid biomembranes." J Phys Condens Matter **12**: A315-20.

Evans, E. and K. Ritchie (1997). "Dynamic strength of molecular adhesion bonds." Biophys J **72**(4): 1541-55.

Evans, E., K. Ritchie, et al. (1995). "Sensitive force technique to probe molecular adhesion and structural linkages at biological interfaces." Biophys J **68**(6): 2580-7.

Fabre, S., N. Reymond, et al. (2002). "Prominent role of the Ig-like V domain in trans-interactions of nectins. Nectin3 and nectin 4 bind to the predicted C-C'-C"-D beta-strands of the nectin1 V domain." J Biol Chem **277**(30): 27006-13.

Farquhar, M. G. and G. E. Palade (1963). "Junctional complexes in various epithelia." J Cell Biol **17**: 375-412.

Grubmuller, H., B. Heymann, et al. (1996). "Ligand binding: molecular mechanics calculation of the streptavidin-biotin rupture force." Science **271**(5251): 997-9.

Gumbiner, B. M. (1996). "Cell adhesion: the molecular basis of tissue architecture and morphogenesis." Cell **84**(3): 345-57.

Gumbiner, B. M. (2000). "Regulation of cadherin adhesive activity." J Cell Biol **148**(3): 399-404.

Gumbiner, B. M. (2005). "Regulation of cadherin-mediated adhesion in morphogenesis." Nat Rev Mol Cell Biol **6**(8): 622-34.

He, W., P. Cowin, et al. (2003). "Untangling desmosomal knots with electron tomography." Science **302**(5642): 109-13.

Honda, T., K. Shimizu, et al. (2003). "Antagonistic and agonistic effects of an extracellular fragment of nectin on formation of E-cadherin-based cell-cell adhesion." Genes Cells **8**(1): 51-63.

Irie, K., K. Shimizu, et al. (2004). "Roles and modes of action of nectins in cell-cell adhesion." Semin Cell Dev Biol **15**(6): 643-56.

Ishijima, A., T. Doi, et al. (1991). "Sub-piconewton force fluctuations of actomyosin in vitro." Nature **352**(6333): 301-6.

Ishijima, A., H. Kojima, et al. (1996). "Multiple- and single-molecule analysis of the actomyosin motor by nanometer-piconewton manipulation with a microneedle: unitary steps and forces." Biophys J **70**(1): 383-400.

Kishino, A. and T. Yanagida (1988). "Force measurements by micromanipulation of a single actin filament by glass needles." Nature **334**(6177): 74-6.

Kitagawa, M., M. Natori, et al. (2000). "Mutation analysis of cadherin-4 reveals amino acid residues of EC1 important for the structure and function." Biochem Biophys Res Commun **271**(2): 358-63.

Kitamura, K., M. Tokunaga, et al. (2005). "Mechanism of muscle contraction based on stochastic properties of single actomyosin motors observed in vitro." BIOPHYSICS **1**: 1-19.

Kitamura, K., M. Tokunaga, et al. (1999). "A single myosin head moves along an actin filament with regular steps of 5.3 nanometres." Nature **397**(6715): 129-34.

Klingelhofer, J., O. Y. Laur, et al. (2002). "Dynamic interplay between

adhesive and lateral E-cadherin dimers." Mol Cell Biol **22**(21): 7449-58.

Kramers, H. A. (1940). "Brownian motion in a field of force and the diffusion model of chemical reactions." Physica 7(4): 284-304.

Krummenacher, C., I. Baribaud, et al. (2002). "Effects of herpes simplex virus on structure and function of nectin-1/HveC." J Virol **76**(5): 2424-33.

Laur, O. Y., J. Klingelhofer, et al. (2002). "Both the dimerization and immunochemical properties of E-cadherin EC1 domain depend on Trp(156) residue." Arch Biochem Biophys **400**(1): 141-7.

Lopez, M., M. Aoubala, et al. (1998). "The human poliovirus receptor related 2 protein is a new hematopoietic/endothelial homophilic adhesion molecule." Blood **92**(12): 4602-11.

Ludwig, F. and E. Evans (2000). "How strong is molecular anchoring in biomembranes?" BIF Futura **15**: 96-103.

Marshall, B. T., M. Long, et al. (2003). "Direct observation of catch bonds involving cell-adhesion molecules." Nature **423**(6936): 190-3.

Martinez-Rico, C., F. Pincet, et al. (2005). "Separation force measurements reveal different types of modulation of E-cadherin-based adhesion by

nectin-1 and -3." J Biol Chem **280**(6): 4753-60.

Merkel, R., P. Nassoy, et al. (1999). "Energy landscapes of receptor-ligand bonds explored with dynamic force spectroscopy." Nature **397**(6714): 50-3.

Miyahara, M., H. Nakanishi, et al. (2000). "Interaction of nectin with afadin is necessary for its clustering at cell-cell contact sites but not for its cis dimerization or trans interaction." J Biol Chem **275**(1): 613-8.

Mizoguchi, A., H. Nakanishi, et al. (2002). "Nectin: an adhesion molecule involved in formation of synapses." J Cell Biol **156**(3): 555-65.

Momose, Y., T. Honda, et al. (2002). "Role of the second immunoglobulin-like loop of nectin in cell-cell adhesion." Biochem Biophys Res Commun **293**(1): 45-9.

Nagafuchi, A. (2001). "Molecular architecture of adherens junctions." Curr Opin Cell Biol **13**(5): 600-3.

Nagar, B., M. Overduin, et al. (1996). "Structural basis of calcium-induced E-cadherin rigidification and dimerization." Nature **380**(6572): 360-4.

Nose, A., K. Tsuji, et al. (1990). "Localization of specificity determining sites in cadherin cell adhesion molecules." Cell **61**(1): 147-55.

Ozaki-Kuroda, K., H. Nakanishi, et al. (2002). "Nectin couples cell-cell adhesion and the actin scaffold at heterotypic testicular junctions." Curr Biol **12**(13): 1145-50.

Ozawa, M. (2002). "Lateral dimerization of the E-cadherin extracellular domain is necessary but not sufficient for adhesive activity." J Biol Chem **277**(22): 19600-8.

Ozawa, M. and R. Kemler (1998). "The membrane-proximal region of the E-cadherin cytoplasmic domain prevents dimerization and negatively regulates adhesion activity." J Cell Biol **142**(6): 1605-13.

Perret, E., A. M. Benoliel, et al. (2002). "Fast dissociation kinetics between individual E-cadherin fragments revealed by flow chamber analysis." Embo J **21**(11): 2537-46.

Perret, E., A. Leung, et al. (2004). "Trans-bonded pairs of E-cadherin exhibit a remarkable hierarchy of mechanical strengths." Proc Natl Acad Sci U S A **101**(47): 16472-7.

Pertz, O., D. Bozic, et al. (1999). "A new crystal structure, Ca2+ dependence and mutational analysis reveal molecular details of E-cadherin homoassociation." Embo J **18**(7): 1738-47.

Pokutta, S., K. Herrenknecht, et al. (1994). "Conformational changes of the recombinant extracellular domain of E-cadherin upon calcium binding." Eur J Biochem **223**(3): 1019-26.

Renaud-Young, M. and W. J. Gallin (2002). "In the first extracellular domain of E-cadherin, heterophilic interactions, but not the conserved His-Ala-Val motif, are required for adhesion." J Biol Chem **277**(42): 39609-16.

Reymond, N., S. Fabre, et al. (2001). "Nectin4/PRR4, a new afadin-associated member of the nectin family that trans-interacts with nectin1/PRR1 through V domain interaction." J Biol Chem **276**(46): 43205-15.

Satoh-Horikawa, K., H. Nakanishi, et al. (2000). "Nectin-3, a new member of immunoglobulin-like cell adhesion molecules that shows homophilic and heterophilic cell-cell adhesion activities." J Biol Chem **275**(14): 10291-9.

Shan, W. S., H. Tanaka, et al. (2000). "Functional cis-heterodimers of N- and R-cadherins." J Cell Biol **148**(3): 579-90.

Shapiro, L., A. M. Fannon, et al. (1995). "Structural basis of cell-cell adhesion by cadherins." Nature **374**(6520): 327-37.

Silvius, J. R. and M. J. Zuckermann (1993). "Interbilayer transfer of phospholipid-anchored macromolecules via monomer diffusion." Biochemistry **32**(12): 3153-61.

Sivasankar, S., W. Brieher, et al. (1999). "Direct molecular force measurements of multiple adhesive interactions between cadherin ectodomains." Proc Natl Acad Sci U S A **96**(21): 11820-4.

Strunz, T., K. Oroszlan, et al. (1999). "Dynamic force spectroscopy of single DNA molecules." Proc Natl Acad Sci U S A **96**(20): 11277-82.

Tachibana, K., H. Nakanishi, et al. (2000). "Two cell adhesion molecules, nectin and cadherin, interact through their cytoplasmic domain-associated proteins." J Cell Biol **150**(5): 1161-76.

Takahashi, K., H. Nakanishi, et al. (1999). "Nectin/PRR: an immunoglobulin-like cell adhesion molecule recruited to cadherin-based adherens junctions through interaction with Afadin, a PDZ domain-containing protein." J Cell Biol **145**(3): 539-49.

Takai, Y. and H. Nakanishi (2003). "Nectin and afadin: novel organizers of intercellular junctions." J Cell Sci **116**(Pt 1): 17-27.

Takeda, H., Y. Shimoyama, et al. (1999). "E-cadherin functions as a cis-dimer

at the cell-cell adhesive interface in vivo." Nat Struct Biol **6**(4): 310-2.

Takeichi, M. (1991). "Cadherin cell adhesion receptors as a morphogenetic regulator." Science **251**(5000): 1451-5.

Tamura, K., W. S. Shan, et al. (1998). "Structure-function analysis of cell adhesion by neural (N-) cadherin." Neuron **20**(6): 1153-63.

Tepass, U., K. Truong, et al. (2000). "Cadherins in embryonic and neural morphogenesis." Nat Rev Mol Cell Biol **1**(2): 91-100.

Tokunaga, M., T. Aoki, et al. (1997). "Subpiconewton intermolecular force microscopy." Biochem Biophys Res Commun **231**(3): 566-9.

Troyanovsky, S. (2005). "Cadherin dimers in cell-cell adhesion." Eur J Cell Biol **84**(2-3): 225-33.

Tsukita, S. and M. Furuse (1999). "Occludin and claudins in tight-junction strands: leading or supporting players?" Trends Cell Biol **9**(7): 268-73.

Tsukita, S., M. Furuse, et al. (2001). "Multifunctional strands in tight junctions." Nat Rev Mol Cell Biol **2**(4): 285-93.

Tsukita, S., A. Nagafuchi, et al. (1992). "Molecular linkage between cadherins and actin filaments in cell-cell adherens junctions." Curr Opin Cell Biol **4**(5): 834-9.

Vleminckx, K. and R. Kemler (1999). "Cadherins and tissue formation: integrating adhesion and signaling." Bioessays **21**(3): 211-20.

Yagi, T. and M. Takeichi (2000). "Cadherin superfamily genes: functions, genomic organization, and neurologic diversity." Genes Dev **14**(10): 1169-80.

Yasumi, M., K. Shimizu, et al. (2003). "Role of each immunoglobulin-like loop of nectin for its cell-cell adhesion activity." Biochem Biophys Res Commun **302**(1): 61-6.

Zhu, B., S. Chappuis-Flament, et al. (2003). "Functional analysis of the structural basis of homophilic cadherin adhesion." Biophys J **84**(6): 4033-42.

Zhu, C., M. Long, et al. (2002). "Measuring receptor/ligand interaction at the single-bond level: experimental and interpretative issues." Ann Biomed Eng **30**(3): 305-14.

8. Activities

(1) 学術雑誌等（紀要・論文集等も含む）に発表した論文又は著書

1) ○Yoshikazu Tsukasaki[1], Kazuo Kitamura[2], Kazuya Shimizu[3], Iwane H. Atsuko[4], Yoshimi Takai[5], Toshio Yanagida[6]

Role of multiple bonds between the single cell adhesion molecules, nectin and cadherin, revealed by high sensitive force measurements

Journal of Molecular Biology, 367: 996-1006, 2007

2) ○Yoshikazu Tsukasaki[1], Kazuo Kitamura[2], Kazuya Shimizu[3], Iwane H. Atsuko[4], Yoshimi Takai[5], Toshio Yanagida[6]

Single Molecule Interactions Between Cell Adhesion Molecules, Nectin and Cadherin, Probed By Intermolecular Force Microscopy

Cell Structure and Function supplement, vol. 29, 41, 2004

3) ○Yoshikazu Tsukasaki[1], Kazuo Kitamura[2], Kazuya Shimizu[3], Iwane H. Atsuko[4], Yoshimi Takai[5], Toshio Yanagida[6]

Direct Observation of Molecular Recognition Between Cell adhesion Molecules Using Flexible Glass Microneedle.

Nanotech Insight supplement, 189, 2005

4) ○Yoshikazu Tsukasaki[1], Kazuo Kitamura[2], Kazuya Shimizu[3], Iwane H. Atsuko[4], Yoshimi Takai[5], Toshio Yanagida[6]

Direct Observation of Biomolecule Nano-reaction-field Using Flexible Glass Microneedle.

Biophysical Journal supplement, vol. 90, 33a, 2006

(2) 国際会議における発表

1) ○Yoshikazu Tsukasaki[1], Kazuo Kitamura[2], Kazuya Shimizu[3], Iwane H. Atsuko[4], Yoshimi Takai[5], Toshio Yanagida[6]

Single molecule Interactions between cell adhesion molecules, Nectin and Cadherin, Probed by Intermolecular Force Microscopy

The 57th Annual Meeting of Japan Society for Cell Biology; Senri Life Science Center, Osaka, Japan, May 26-28, 2004

2) ○Yoshikazu Tsukasaki[1], Kazuo Kitamura[2], Kazuya Shimizu[3], Iwane H. Atsuko[4], Yoshimi Takai[5], Toshio Yanagida[6]

Novel stable interactions between cell adhesion molecules detected using intermolecular force microscopy at sub-piconewton resolution.

The 10th International Workshop on "Single Molecule Detection and Ultrasensitive Analysis in Life Sciences"; WISTA Campus, Berlin-Aldlershof, Germany, September 22-24, 2004

3) ○Yoshikazu Tsukasaki[1], Kazuo Kitamura[2], Kazuya Shimizu[3], Iwane H. Atsuko[4], Yoshimi Takai[5], Toshio Yanagida[6]

Direct Observation of Biomolecule Nano-reaction-field Using Flexible Intermolecular Force Microscopy.

The International Conference on Nanotechnology: Science and Application (Nanotech Insight 2005); Luxor, Egypt, February 20-25, 2005

4) ○Yoshikazu Tsukasaki[1], Kazuo Kitamura[2], Kazuya Shimizu[3], Iwane H. Atsuko[4], Yoshimi Takai[5], Toshio Yanagida[6]

Direct Observation of Molecular Recognition Between Cell adhesion Molecules Using Flexible Glass Microneedle.

The 50th Annual Meeting of Biophysical Society; Salt Lake City Convention

Facilities, Utah, Japan, February 18-22, 2006

(3) 国内学会・シンポジウム等における発表

1) ○塚崎克和[1]、喜多村和郎[2]、清水一也[3]、岩根敦子[4]、高井義美[5]、柳田敏雄[6]

分子間力顕微鏡を用いた細胞間の接着形成システムに関与する接着蛋白質の1分子物性計測

第41回日本生物物理学会　於朱鷺メッセ新潟コンベンションセンター

2003年9月23～25日

2) ○塚崎克和[1]、喜多村和郎[2]、清水一也[3]、岩根敦子[4]、高井義美[5]、柳田敏雄[6]

高感度分子間力顕微鏡により検出された細胞間接着分子の新しい分子認識メカニズム

第42回日本生物物理学会　於国立京都国際会館　2004年12月13～15日

3) ○塚崎克和[1]、喜多村和郎[2]、清水一也[3]、岩根敦子[4]、高井義美[5]、柳

田敏雄[6]

高感度1 分子相互作用計測により検出された細胞間接着分子ダイナミクス

第27回日本分子生物学会　於神戸ポートピアホテル　2004年12月18～11日

4) ○塚崎克和[1]、喜多村和郎[2]、清水一也[3]、岩根敦子[4]、高井義美[5]、柳田敏雄[6]

高感度分子間力顕微鏡により検出された細胞間接着分子の新しい分子認識メカニズム

生体運動研究合同班会議　於千里ライフサイエンスセンター　2005年1月7～9日

5) ○塚崎克和[1]、喜多村和郎[2]、清水一也[3]、岩根敦子[4]、高井義美[5]、柳田敏雄[6]

高感度分子間力顕微鏡による生体分子間ナノ反応場の1分子直接観察

第3回ナノ学会　於仙台市民会館　2005年5月8～10日

6) ○塚崎克和[1]、喜多村和郎[2]、清水一也[3]、岩根敦子[4]、高井義美[5]、柳田敏雄[6]

高感度分子間力顕微鏡による細胞間接着分子間ナノ反応場の１分子直接観察

第 43 回日本生物物理学会　於札幌コンベンションセンター　2005 年 11 月 23～25 日

7) ○森松賢順[7]、西川宗[8]、塚崎克和[1]、岡田拓也[8]、岩根敦子[4]、柳田敏雄[6]

ガラスニードルを用いたミオシンの変位計測の簡便化

第 43 回日本生物物理学会　於札幌コンベンションセンター　2005 年 11 月 23～25 日

著者の身分

[1]特別研究員 DC2（奈良先端大）、[2]海外特別研究員（ロンドン大学）、[3]研究員（神戸大）、[4]助手（阪大）、[5]教授（阪大）、[6]教授（阪大）、[7]大学院生（阪大）、[8]研究員（科学技術振興機構）

9. Acknowledgements

本学位論文を執筆するに当たり、お世話になりましたすべての方々に感謝致します。

山下一郎教授、柳田敏雄教授、高井義美教授には、常日頃から御助言、御指導いただきました。深く感謝致します。

菊池純一教授、片岡幹雄教授、谷原正夫教授には、大変お忙しい中で、本学位論文の審査をしていただきました。深く感謝致します。

喜多村和郎助手には、ガラスマイクロニードル法のイロハを伝授していただきました。深く感謝致します。何も知らなかった私が現在こうして博士論文を提出できるのも本技術のおかげであり、今後、絶やさぬよう精錬・発展させていく所存でございます。

岩根敦子助教授、扇田久和助手、清水一也博士には、研究全般に対して多大な御助言、御指導をいただきました。深く感謝致します。

奈良先端科学技術大学院大学物質創成研究科メゾスコピック物質科学講座、大阪大学生命機能研究科ナノ生体科学講座のメンバー、特に同期生でもあり友人である宮永之寛君、高橋正裕君、先輩である高木拓明博士、有賀隆行博士、小塚淳博士、谷口雄一博士、岩城光宏博士、渡邉朋信助手には、日頃から有益な議論をしていただきました。彼らとの議論から得た何物にも変え難い財産は、これからの研究に生かしていきたいと思います。深く感謝致します。

最後に、２０代後半まで、学びの機会を提供してくださいました、父、母、そして家族に感謝申し上げます。

２００７年１月

塚崎　克和

高感度分子間力顕微鏡による細胞間接着分子ネクチン・カドヘリンの１分子間結合力計測

Bond strength measurement between the single cell adhesion molecules, nectin and cadherin, using high sensitive Intermolecular Force Microscopy

Department of Mesoscopic Materials Science, Graduate School of Materials Science, Nara Institute of Science and Technology

Doctoral dissertation Jan, 2007

Yoshikazu Tsukasaki